Journal of Inorganic Biochemistry 282 (2026) 113344

Contents lists available at ScienceDirect

Journal of Inorganic Biochemistry

journal homepage: www.elsevier.com/locate/jinorgbio

Design, synthesis and photocatalytic activities of functionalized Re(I) bipyridine tricarbonyl complexes toward CO_2 reduction and carboxylation

Phurinat Lorwongkamol [a], Yutaka Saga [a,b,*], Tetsuya Kambe [a,c], Mio Kondo [d], Shigeyuki Masaoka [a,b,*]

[a] Division of Applied Chemistry, Graduate School of Engineering, The University of Osaka, 2-1 Yamadaoka, Suita, Osaka 565-0871, Japan
[b] Innovative Catalysis Science Division, Institute for Open and Transdisciplinary Research Initiatives (ICS-OTRI), The University of Osaka, 2-1 Yamadaoka, Suita, Osaka 565-0871, Japan
[c] Department of Chemistry, Institute of Pure and Applied Sciences, University of Tsukuba, 1-1-1 Tennodai, Tsukuba, Ibaraki 305-8577, Japan
[d] Department of Chemistry, School of Science, Institute of Science Tokyo, 2-12-1 Ookayama, Meguro-ku, Tokyo 152-8551, Japan

ARTICLE INFO

Keywords:
Rhenium complex
Photocatalysis
CO_2 reduction
Carboxylation
Functionalized ligands

ABSTRACT

Natural metalloenzymes efficiently catalyze chemical transformations by precisely controlling the local environment around the active site, thereby enabling selective substrate activation and reaction control. This general concept has motivated extensive efforts to improve molecular catalysts by ligand modification and functionalization. In this work, we designed and synthesized functionalized derivatives of the *fac*-Re(2,2′-bipyridine)$(CO)_3Cl$ complex (**Re-1**), which has long been recognized as a benchmark catalyst for photochemical CO_2 reduction, and which we have recently demonstrated to also catalyze the carboxylation of organic substrates with CO_2. Using these complexes, we investigated how substituents on the bipyridine ligand affect photocatalytic activities in both CO_2 reduction and carboxylation reactions. All new complexes were fully characterized by single-crystal X-ray diffraction analysis as well as by spectroscopic and electrochemical methods. The introduction of electron-withdrawing functional groups induces clear changes in the electronic structures of the complexes, as evidenced by redshifts in their absorption spectra, CO stretching frequencies, and reduction potentials. In photocatalytic CO_2 reduction, the catalytic activities of the functionalized complexes depend strongly on these electronic properties, whereas in carboxylation reactions, all complexes show comparable catalytic performance regardless of the nature of the functional groups. Moreover, the present system also exhibits additional reactivities, including [2 + 2] dimerization and hydroacylation reactions. Collectively, this work reports the design, synthesis, and characterization of a new series of functionalized Re(I) complexes, and provides a useful experimental basis for understanding how ligand modification influences their properties and reactivity, thereby offering guidance for future development of Re-based molecular systems for CO_2 utilization.

1. Introduction

Carbon dioxide (CO_2) is one of the most abundant and yet chemically inert carbon resources on Earth. In nature, however, CO_2 is efficiently captured, activated, and converted into organic molecules by metalloenzymes under ambient temperature and pressure [1,2]. Such remarkable reactivity is enabled not only by the metal active sites but also by the precisely organized secondary coordination sphere, which stabilizes key intermediates and promotes multistep transformations. Representative examples include [NiFe] carbon monoxide dehydrogenase (CODH) [2–4] and formate dehydrogenase (FDH) [5,6]. In CODH, CO_2 binds to a reduced Ni center through the carbon atom while interacting with a nearby Fe site and surrounding residues, where hydrogen bonding and local proton sources assist in stabilizing key intermediates. In FDH, Mo or W centers activate CO_2 through coordination with an oxygen atom and proton transfer facilitated by nearby amino acid residues that control substrate orientation and proton delivery. These examples highlight how secondary coordination sphere interactions, electronic modulation of the metal active site, and local substrate accumulation cooperatively enable efficient CO_2 conversion

* Corresponding authors at: Division of Applied Chemistry, Graduate School of Engineering, The University of Osaka, 2-1 Yamadaoka, Suita, Osaka 565-0871, Japan.
E-mail addresses: ysaga@chem.eng.osaka-u.ac.jp (Y. Saga), masaoka@chem.eng.osaka-u.ac.jp (S. Masaoka).

https://doi.org/10.1016/j.jinorgbio.2026.113344
Received 2 February 2026; Received in revised form 15 April 2026; Accepted 29 April 2026
Available online 5 May 2026

under mild conditions. Inspired by these sophisticated biological systems, extensive efforts have been devoted to the development of coordination compounds with functional ligands as catalysts for small molecule conversions or chemical transformations [7,8].

In the context of CO_2 photoreduction catalysis, *fac*-Re(2,2′-bipyridine)$(CO)_3Cl$ (**Re-1**) occupies a unique and historically important position (Fig. 1a). Since its first report in 1983 as a molecular photocatalyst for the reduction of CO_2 to CO [9], **Re-1** has been recognized as a benchmark platform that integrates photosensitization and catalytic functions within a single molecular framework. Owing to its favorable photophysical properties, high chemical stability and structural flexibility, **Re-1** and its derivatives have been extensively studied and structurally modified to improve catalytic performance, or be incorporated into functional materials [10–27].

Despite this long history and significant advances in the CO_2 reduction, the application of Re complexes to reactions other than CO_2 reduction remains largely unexplored. Very recently, we reported the first clear demonstration of **Re-1** as a catalyst for visible-light-driven carboxylation of an organic substrate with CO_2 (Fig. 1b) [28]. This catalytic system enabled the selective formation of carboxylic acids with a turnover number of up to 2600 and excellent regioselectivity. Notably, the competing CO formation pathway was completely suppressed. Mechanistic studies and control experiments revealed that a Re-CO_2 adduct, in which CO_2 is activated on the Re metal center, plays a key role in the productive carboxylation process. This work established a fundamentally new reactivity and application of Re(I) diimine complexes, not merely as CO_2 reduction catalysts, but as versatile platforms for CO_2 utilization in organic synthesis.

Encouraged by this conceptual advance, we set out to further expand the catalytic potential of Re(I) bipyridine tricarbonyl complex platform by introducing functional groups onto the bipyridine ligand of **Re-1** (Fig. 1c). In this context, previous studies have demonstrated that incorporating functional groups into ligand frameworks can significantly influence catalytic behavior through secondary coordination sphere effects. For example, hydrogen-bonding groups, such as hydroxyl [11,29] and thiourea [30] groups, can stabilize metal-CO_2 intermediates, while charged substituents can modulate local electrostatic environments and redox properties [27,31,32]. In Re, Mn and related systems, such modifications have enabled control over catalytic activity, overpotential, and product selectivity. Notable examples include imidazolium-functionalized systems [33–36], as well as amine-containing ligands [37,38] that act as proton relays or electrostatic stabilizers. These studies collectively demonstrate the importance of ligand design in tuning catalytic performance.

In this work, we report the design, synthesis, and catalytic application of a series of new Re complexes bearing carboxyl (**Re-2**), hydroxy (**Re-3**), imidazolium (**Re-4**), and amino (**Re-5**) functional groups (Fig. 2). Our molecular design was guided by two hypotheses to enhance the reactivity for CO_2 utilization. The first hypothesis is the stabilization of CO_2 bound on Re metal center or reaction intermediates, which is expected to lower the activation barrier and facilitate the reaction progress. The second hypothesis is the promotion of CO_2 capture and accumulation in the vicinity of the metal center, by the ancillary ligand, thereby increasing the effective rate of CO_2 binding to the catalyst [7,11,35,39,40].

Based on these design hypotheses, we selected four types of functional groups with distinct roles. We anticipate that the carboxyl groups in **Re-2** and the hydroxy groups in **Re-3** could act as hydrogen-bonding donors to stabilize the Re-CO_2 intermediate. The positively charged imidazolium groups in **Re-4** were designed to provide electrostatic stabilization to the negatively charged Re-CO_2 adduct. In addition, the deprotonation of the imidazolium group to generate carbene species could enable the nucleophilic CO_2 capture and thereby increase the local concentration of CO_2 around the Re center [41]. Finally, the primary amino groups in **Re-5** were envisioned to serve not only as hydrogen-bonding donors but also CO_2-capturing moieties through the reversible formation of carbamate species [42,43]. In the context of alkene carboxylation, our previous mechanistic studies suggest that a two-

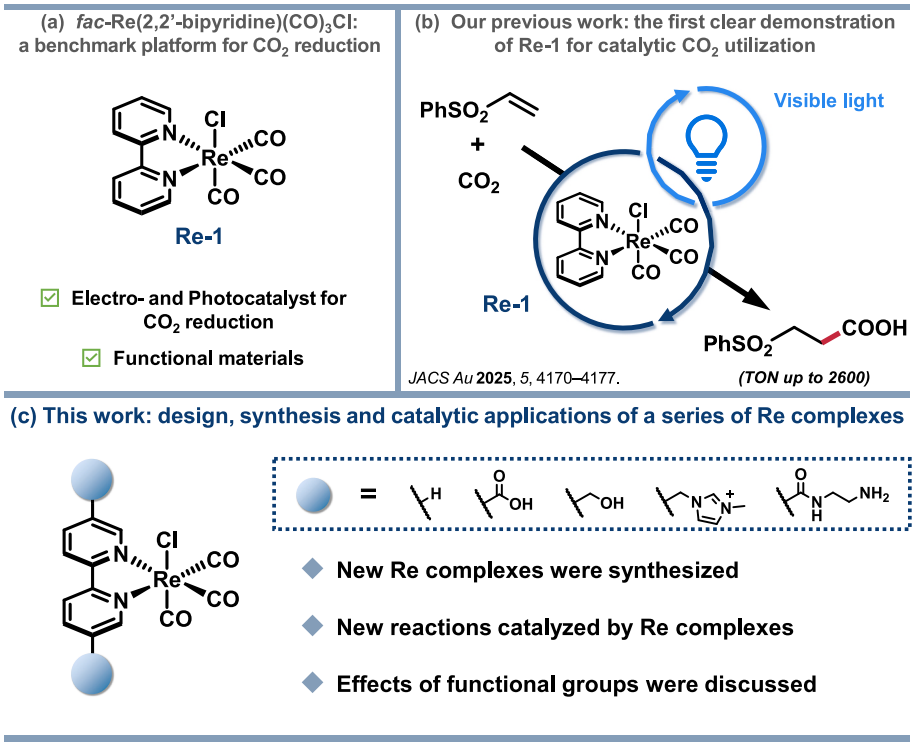

Fig. 1. (a) *fac*-Re(2,2′-bipyridine)$(CO)_3Cl$ (**Re-1**) as a benchmark molecular platform for photocatalytic reduction of CO_2 to CO. (b) Our previous work: the first clear demonstration of **Re-1** as a catalyst for CO_2 utilization other than CO_2 reduction. (c) This work: design, synthesis and catalytic application of a series of new Re complexes.

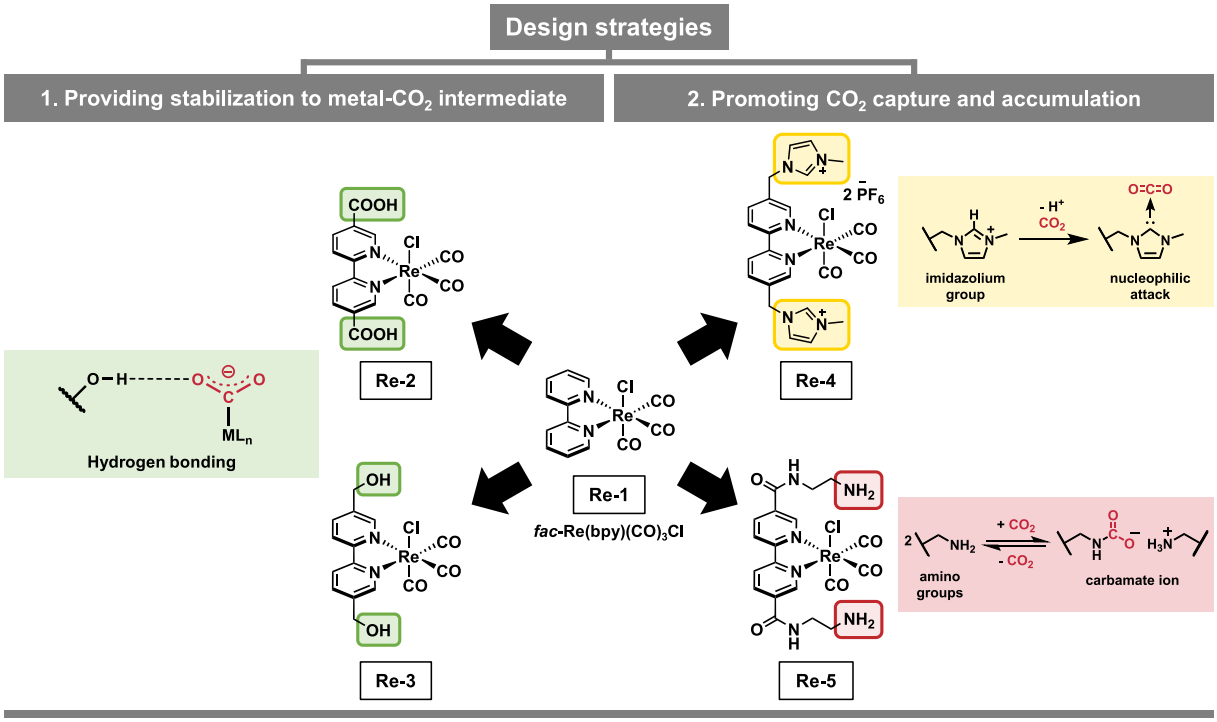

Fig. 2. Design strategies for the development of new Re complexes by introducing various functional groups onto the 2,2′-bipyridine ligand.

electron-reduced Re center interacts with CO_2 to form a nucleophilic Re-CO_2 adduct, which subsequently reacts with the organic substrate [28]. In this system, no additional functional groups are present to assist CO_2 capture or stabilization, and therefore ligand-based functionalization is expected to play an important role in facilitating the reaction. Based on these considerations, we introduced carboxyl (**Re-2**), hydroxy (**Re-3**), imidazolium (**Re-4**), and amino (**Re-5**) functional groups onto the bipyridine ligand.

All new complexes were unambiguously characterized by single-crystal X-ray diffraction analysis. Their photophysical and electrochemical properties were investigated and compared, elucidating the electronic effects of the functional groups. Furthermore, the reactivities of these complexes were comprehensively examined, revealing not only photocatalytic CO_2 reduction and carboxylation with CO_2, but also additional reaction pathways, such as [2 + 2] dimerization and hydroacylation reactions. While pronounced differences in catalytic activity were observed for CO_2 reduction to CO, all complexes exhibited comparable efficiencies in the carboxylation reaction. Although the functional groups were initially designed to exert secondary coordination sphere effects, structural analysis revealed that these groups are located relatively far from the metal center, indicating that direct interaction with CO_2-bound intermediates is likely limited under the present structural constraints. Accordingly, the initially proposed roles of these functional groups are not fully realized in the present system, while providing insight into the structural requirements for effective secondary coordination sphere interactions in such systems.

Overall, these results show that CO_2 reduction is influenced by the electronic properties of the complexes, whereas in the carboxylation reaction the present complexes display similar performance across different ligand environments. Collectively, this work demonstrates that simple ligand modification of a benchmark Re(I) complex provides a useful framework for studying how structural changes influence properties and reactivity, and for guiding future development of Re-based systems for CO_2 utilization.

2. Experimental

2.1. Synthesis of 2,2′-bipyridine derivatives

Diethyl [2,2′-bipyridine] -5,5′-dicarboxylate (L3a). The synthesis followed a reported procedure with slight modifications [44]. In a 50-mL-round-bottom flask containing 2,2′-bipyridine-5,5′-dicarboxylic acid (200 mg, 0.819 mmol) and ethanol (10 mL) was added concentrated H_2SO_4 (1.5 mL) dropwise, and the mixture was refluxed under a N_2 atmosphere overnight. Then, the solvent was removed under reduced pressure, and the resulting residue was neutralized with a saturated solution of $NaHCO_3$. The mixture was extracted with $CHCl_3$, and the combined organic phase was evaporated under reduced pressure to afford **L3a** as a white solid. Yield: 195.1 mg (78%) ^{1}H NMR (400 MHz, $CDCl_3$) δ: 9.30 (2H, d, $J = 2.0$ Hz), 8.58 (2H, d, $J = 8.4$ Hz), 8.44 (2H, dd, $J = 8.4$, 2.4 Hz), 4.45 (4H, q, $J = 7.2$ Hz), 1.45 (6H, t, $J = 7.2$ Hz). ^{13}C NMR (100 MHz, $CDCl_3$) δ: 165.2, 158.2, 150.6, 138.1, 126.5, 121.2, 61.5, 14.3.

5,5′-bis(hydroxymethyl)-2,2′-bipyridine (L3b). The synthesis followed a reported procedure with slight modifications [44]. The obtained ester **(L3a)** (153 mg, 0.51 mmol) was dissolved in ethanol (12 mL) and the solution was cooled in an ice bath. Then, $NaBH_4$ (259 mg, 6.85 mmol) was slowly added to the solution, and the mixture was refluxed under a N_2 atmosphere overnight. After the reaction, ethanol was removed under reduced pressure and the residue was neutralized with a saturated solution of NH_4Cl. The mixture was extracted with ethyl acetate, and the combined organic phase was evaporated under reduced pressure to afford **L3b** as a yellow solid. Yield: 98.8 mg (90%) ^{1}H NMR (400 MHz, DMSO-d_6) δ: 8.61 (2H, s), 8.34 (2H, d, $J = 8.0$ Hz), 7.86 (2H, dd, $J = 8.0$, 1.6 Hz), 5.40 (2H, t, $J = 5.6$ Hz), 4.59 (4H, d, $J = 6.0$ Hz). ^{13}C NMR (100 MHz, DMSO-d_6) δ: 154.0, 147.7, 138.0, 135.5, 119.9, 60.5.

5,5′-bis(bromomethyl)-2,2′-bipyridine (L4a). The synthesis followed a reported procedure with slight modifications [45]. In an oven dried 50-mL Schlenk tube was added 5,5′-dimethyl-2,2′-bipyridine, (200

mg, 1.09 mmol), *N*-bromosuccinimide (NBS, 425 mg, 2.39 mmol), azobisisobutyronitrile (AIBN, 17.9 mg, 0.11 mmol), and dried CCl_4 (10 mL), then the mixture was refluxed under a N_2 atmosphere overnight. The crude mixture was filtered, and the remaining precipitate was washed thoroughly with CCl_4 after which the combined solution was concentrated and recrystallized from CCl_4 to afford **L4a** as a white solid. Yield: 163.4 mg (46%). ^{1}H NMR (400 MHz, $CDCl_3$) δ: 8.68 (2H, s), 8.40 (2H, d, $J = 8.0$ Hz), 7.86 (2H, dd, $J = 8.0$, 1.2 Hz), 4.54 (4H, s). ^{13}C NMR (100 MHz, $CDCl_3$) δ: 155.4, 149.4, 137.6, 133.9, 121.1, 29.6.

1,1′-([2,2′-bipyridine]-5,5′-diylbis(methylene))bis(3-methyl-1H-imidazol-3-ium)·$(PF_6)_2$ (L4b). The synthesis followed a reported procedure with slight modifications [36]. The obtained product **L4a** (75 mg, 0.22 mmol) was then added into a 50-mL Schlenk tube with 1-methylimidazole (144 mg, 1.75 mmol) and acetonitrile (10 mL). The mixture was degassed with a stream of N_2 gas for 10 min., then refluxed under a N_2 atmosphere overnight. After the reaction, the mixture was evaporated and re-dissolved in $CHCl_3$ (10 mL). The organic layer was extracted with water (5 mL, 5 times). The aqueous phase was collected and concentrated under reduced pressure until the volume was reduced by half. A saturated solution of NH_4PF_6 was added to afford the white precipitate, which was then collected by vacuum filtration, washed with water followed by diethyl ether, and dried under vacuum to afford **L4b** as a white solid. Yield: 60.7 mg (43%). ^{1}H NMR (400 MHz, DMSO-d_6) δ: 9.23 (2H, s), 8.77 (2H, d, $J = 1.6$ Hz), 8.41 (2H, d, $J = 8.0$ Hz), 7.99 (2H, dd, $J = 8.0$, 2.0 Hz), 7.84 (2H, s), 7.73 (2H, s), 5.54 (4H, s), 3.86 (6H, s). ^{13}C NMR (100 MHz, DMSO-d_6) δ: 154.9, 149.4, 137.6, 137.0, 131.3, 124.2, 122.4, 120.7, 49.2, 36.0.

Di-tert-butyl (((([2,2′-bipyridine]-5,5′-dicarbonyl)bis(azanediyl))bis(ethane-2,1-diyl))dicarbamate (L5). The synthesis followed a reported procedure with slight modifications [46]. In a 50-mL round-bottom flask was added 5,5′-dicarboxylic acid-2,2′-bipyridine (300 mg, 1.23 mmol), dimethylformamide (DMF) (10 mL), 1-[Bis(dimethylamino)methylene]-1H-1,2,3-triazolo[4,5-*b*]pyridinium 3-Oxide Hexafluorophosphate (HATU) (934 mg, 2.46 mmol), and *N*,*N*-diisopropylethylamine (0.7 mL, 4.02 mmol), and the mixture was stirred under a N_2 atmosphere for 10 min. Then, a 5-mL DMF solution of *N*-(*tert*-butoxycarbonyl)-1,2-diaminoethane (433 mg, 2.70 mmol) was added and the mixture was stirred under an N_2 atmosphere for another 2 h. Then, the mixture was diluted with water to immediately give a white precipitate. The precipitate was collected by vacuum filtration, washed with water, and dried under vacuum to afford **L5** as a white solid. Yield: 591.8 mg (91%). ^{1}H NMR (400 MHz, DMSO-d_6) δ: 9.11 (2H, s), 8.78 (2H, t, $J = 5.6$ Hz), 8.51 (2H, d, $J = 8.0$ Hz), 8.36 (2H, dd, $J = 8.0$, 1.6 Hz), 6.97 (2H, t, $J = 5.6$ Hz), 3.14 (4H, q, $J = 5.6$ Hz), 1.37 (18H, s). ^{13}C NMR (100 MHz, DMSO-d_6) δ: 164.6, 156.2, 155.7, 148.4, 136.1–136.5 (m), 130.3, 120.2–120.6 (m), 77.7, 28.1–28.3 (m). Note that the methylene signals are not clearly observed due to the overlap with the residual solvent signals of DMSO-d_6. Attempts to measure NMR spectra in other solvents were unsuccessful because the compound is insoluble in other solvents other than DMSO.

2.2. Synthesis of Re complexes

Re(2,2′-bipyridine)$(CO)_3$Cl (Re-1). In a 50-mL round-bottom flask was added $Re(CO)_5Cl$ (100 mg, 0.28 mmol), 2,2′-bipyridine (43 mg, 0.28 mmol), and toluene (20 mL). The mixture was refluxed under a N_2 atmosphere for 2 h, then left in a freezer overnight to allow complete precipitation. The resulting solid was obtained by vacuum filtration, washed with diethyl ether, and dried under vacuum to afford a yellow solid. Yield: 122.6 mg (95%). ^{1}H NMR (400 MHz, DMSO-d_6) δ: 9.02 (2H, dd, $J = 5.6$, 1.2 Hz), 8.77 (2H, d, $J = 8.4$ Hz), 8.35 (2H, td, $J = 8.0$, 1.2 Hz), 7.74–7.79 (2H, m). ^{13}C NMR (100 MHz, DMSO-d_6) δ: 197.8, 190.1, 155.2, 153.0, 140.4, 128.0, 124.4. HRMS (ESI): *m/z* calcd for $C_{13}H_8N_2O_3Re$ $[M\text{-}Cl]^+$ 427.0087; found 427.0091 $[M\text{-}Cl]^+$. Anal. Found (calculated for $C_{13}H_8ClN_2O_3Re$): C, 33.70 (33.81); H, 1.85 (1.75); N, 6.02 (6.07).

Re(2,2′-bipyridine-5,5′-dicarboxylic acid)$(CO)_3$Cl (Re-2). In a 100-mL round-bottom flask was added $Re(CO)_5Cl$ (100 mg, 0.28 mmol), 5,5′-dicarboxylic acid-2,2′-bipyridine (67 mg, 0.28 mmol), and a mixture of toluene and methanol (20/10 mL). The mixture was refluxed under a N_2 atmosphere for 3 h, then left in a freezer overnight to allow complete precipitation. The resulting solid was collected by vacuum filtration, washed with hexane, and dried under vacuum to afford an orange solid. Yield: 110.4 mg (74%). Diffraction-quality crystal was grown from the evaporation of diethyl ether into a saturated MeOH solution under low temperature. ^{1}H NMR (400 MHz, DMSO-d_6) δ: 14.37 (1H, brs), 9.33 (2H, d, $J = 2.0$ Hz), 8.98 (2H, d, $J = 8.0$ Hz), 8.75 (2H, dd, $J = 8.0$, 2.0 Hz). ^{13}C NMR (100 MHz, DMSO-d_6) δ: 197.8, 189.2, 164.0, 157.1, 153.0, 140.7, 130.4, 125.5. HRMS (ESI): *m/z* calcd for $C_{15}H_7N_2O_7ClRe$ $[M\text{-}H]^-$ 548.9498; found 548.9505 $[M\text{-}H]^-$. Anal. Found (calculated for $C_{15}H_8ClN_2O_7Re$): C, 32.43 (32.76); H, 1.80 (1.47); N, 4.62 (5.09).

Re(5,5′-bis(hydroxymethyl)-2,2′-bipyridine)$(CO)_3$Cl (Re-3). In a 100-mL round-bottom flask was added $Re(CO)_5Cl$ (100 mg, 0.28 mmol), **L3** (60 mg, 0.28 mmol), and a mixture of toluene and methanol (20/10 mL). The mixture was refluxed under a N_2 atmosphere for 5 h, then the solvent was removed under reduced pressure. The resulting solid was recrystallized from toluene and collected by vacuum filtration, washed with hexane, then dried under vacuum to afford a yellow solid. Yield: 52.5 mg (37%). A diffraction-quality crystal was grown from the evaporation of hexane into a saturated EtOH solution under low temperature. ^{1}H NMR (400 MHz, DMSO-d_6) δ: 8.92 (2H, s), 8.70 (2H, d, $J = 8.8$ Hz), 8.21 (2H, dd, $J = 8.4$, 1.6 Hz), 5.74 (2H, t, $J = 5.6$ Hz), 4.73 (4H, d, $J = 5.6$ Hz). ^{13}C NMR (100 MHz, DMSO-d_6) δ: 197.9, 190.2, 153.7, 150.3, 142.3, 138.0, 123.6, 59.7. HRMS (ESI): *m/z* calcd for $C_{15}H_{12}N_2O_5Re$ $[M\text{-}Cl]^+$ 487.0299; found 487.0317 $[M\text{-}Cl]^+$. Anal. Found (calculated for $C_{15}H_{12}ClN_2O_5Re$): C, 34.46 (34.52); H, 2.53 (2.32); N, 5.29 (5.37).

[Re(1,1′-([2,2′-bipyridine]-5,5′-diylbis(methylene))bis(3-methyl-1H-imidazol-3-ium))$(CO)_3$Cl]$(PF_6)_2$ (Re-4). In a 50-mL round-bottom flask was added $Re(CO)_5Cl$ (28.4 mg, 0.079 mmol), **L4** (50 mg, 0.079 mmol), and a mixture of toluene and methanol (7/3 mL). The mixture was refluxed under a N_2 atmosphere for 2 h. The resulting solid was recrystallized from MeOH/diethyl ether and collected by vacuum filtration, washed with diethyl ether, then dried under vacuum to afford a light yellow solid. Yield: 21.5 mg (28%). A diffraction-quality crystal was grown from the evaporation of diethyl ether into a saturated MeOH solution under low temperature. ^{1}H NMR (400 MHz, DMSO-D_6) δ: 9.27 (2H, s), 9.16 (2H, d, $J = 1.6$ Hz), 8.81 (2H, d, $J = 8.4$ Hz), 8.29 (2H, dd, $J = 8.4$, 1.6 Hz), 7.91 (2H, s), 7.78 (2H, s), 5.69 (4H, s), 3.88 (6H, s). ^{13}C NMR (100 MHz, DMSO-d_6) δ: 197.1, 189.8, 154.7, 152.6, 139.9, 137.4, 135.1, 124.6, 124.3, 122.4, 48.4, 36.0. HRMS (ESI): *m/z* calcd for $C_{23}H_{22}N_6O_3F_6PClRe$ $[M\text{-}PF_6]^+$ 797.0627; found 797.0650 $[M\text{-}PF_6]^+$. Anal. Found (calculated for $C_{23}H_{22}ClF_{12}N_6O_3P_2Re$): C, 29.71 (29.32); H, 2.63 (2.35); N, 9.23 (8.92).

Re(di-tert-butyl (((([2,2′-bipyridine]-5,5′-dicarbonyl)bis(azanediyl))bis(ethane-2,1-diyl))dicarbamate) (Re-5′). In a 50-mL round-bottom flask was added $Re(CO)_5Cl$ (50.0 mg, 0.14 mmol), **L5** (73.1 mg, 0.14 mmol), and toluene (10 mL). The mixture was refluxed under a N_2 atmosphere for 2 h, then left to cool to room temperature. The product was precipitated upon cooling and was collected by vacuum filtration, washed with diethyl ether, and dried under vacuum to afford an orange solid. The obtained product was used in the next step without further purification. Yield: 95.1 mg (84%). ^{1}H NMR (400 MHz, DMSO-d_6) δ: 9.30 (2H, d, $J = 1.6$ Hz), 9.16 (2H, t, $J = 5.6$ Hz), 8.94 (2H, d, $J = 8.4$ Hz), 8.68 (2H, dd, $J = 8.4$, 1.6 Hz), 6.98 (2H, t, $J = 5.6$ Hz), 3.17 (4H, q, $J = 6.0$ Hz), 1.37 (18H, s). MS (ESI): *m/z* calcd for $C_{29}H_{36}N_6O_9NaClRe$ $[M + Na]^+$ 857.17; found 857.58 $[M + Na]^+$.

Re(N^5,$N^{5'}$-bis(2-aminoethyl)-[2,2′-bipyridine]-5,5′-dicarboxamide)$(CO)_3$Cl (Re-5). Deprotection of *tert*-butoxycarbonyl (Boc) groups was performed by mixing the **Re-5′** (72.1 mg, 0.086 mmol) and MeOH (12 mL) in a 50-mL *v*ial followed by adding concentrated hydrochloric acid (7 mL). The mixture was stirred at room temperature during which the deprotection progress was monitored by thin-layer

chromatography (mobile phase: $CHCl_3$/MeOH 19:1 *v*/v). After all the starting material was consumed, the mixture was evaporated and re-dispersed in a solution of MeOH-triethylamine (10 mL/5 mL). The mixture was stirred at room temperature for 30 min. Then evaporated. The resulting solid was washed thoroughly with a solution of $CHCl_3$/triethylamine (100:1 v/v), dried under vacuum, and further purified by recrystallization from MeOH/diethyl ether to afford the orange solid. Yield: 32.9 mg (60%). ^{1}H NMR (400 MHz, DMSO-d_6) δ: 9.50 (2H, brs), 9.33 (2H, d, $J = 1.6$ Hz), 9.00 (2H, d, $J = 8.0$ Hz), 8.86 (2H, dd, $J = 8.4$, 1.6 Hz), 7.51 (2H, brs), 3.58 (4H, brs), 3.02 (4H, t, $J = 5.6$ Hz). ^{13}C NMR (100 MHz, DMSO-d_6) δ: 197.5, 189.6, 163.0, 156.2, 152.1, 138.7, 132.9, 124.7, 38.8, 38.0. HRMS (ESI): *m/z* calcd for $C_{19}H_{20}N_6O_5Re$ $[M\text{-}Cl]^+$ 599.1048; found 599.1056 $[M\text{-}Cl]^+$. Anal. Found (calculated for $C_{19}H_{20}ClN_6O_5Re{\cdot}3.90H_2O$): C, 32.40 (32.71); H, 3.98 (3.55); N, 11.93 (11.53).

2.3. Photocatalytic studies

Photocatalytic CO_2 reduction. A 9-mL glass *v*ial equipped with a stirrer bar were dried under vacuum for 20 min before use. To the vial was added 1,3-Dimethyl-2-phenyl-2,3-dihydro-1*H*-benzo[*d*]imidazole (BIH) (22.4 mg, 0.1 mmol), Re complex (0.001 mmol), and a mixture of DMF and triethanolamine (TEOA) (5:1 *v*/v, 2 mL). Then, the vial was sealed with a rubber septum and the solution was degassed by passing a stream of CO_2 for 20 min. Next, the vial was exposed to a Xenon-are lamp irradiation (300 W, 420-nm long-pass filter) for 3 h, during which the reaction temperature was maintained at 20 °C. The gaseous products were analyzed by gas chromatography. For **Re-4**, a slightly modified preparation was used. In detail, a solution of **Re-4** (0.94 mg, 0.001 mmol) in DMF (1.67 mL) was firstly prepared. Then to this solution was added sodium *tert*-butoxide (0.58 mg, 0.006 mmol), and the mixture was stirred at room temperature for 30 min before TEOA (0.33 mL) and BIH (22.4 mg, 0.1 mmol) were added. Next, the vial was sealed with a rubber septum, and the following steps are identical to the aforementioned procedure.

Photocatalytic carboxylation of phenyl vinyl sulfone with CO_2. A 4-mL glass vial equipped with a stirrer bar were dried under vacuum for 20 min prior to use. To the vial was added phenyl vinyl sulfone (**1**) (16.8 mg, 0.1 mmol), BIH (22.4 mg, 0.1 mmol), Re complex (0.001 mmol), and dimethyl sulfoxide (DMSO) (1 mL). The vial was then sealed with a rubber septum and briefly sonicated to achieve a homogeneous solution. The mixture was degassed by passing a stream of CO_2 for 15 min, then exposed to a Sigma-Aldrich SynLED Parallel Photoreactor (465–470 nm) for 16 h. After 16 h, 1 mL of hydrochloric acid (2.0 M) was added and the mixture was stirred for 30 min at room temperature. The mixture was then extracted with ethyl acetate, dried over sodium sulfate, concentrated under reduced pressure, and dried under vacuum at elevated temperature (60–65 °C). The TON and the regioselectivity of the desired carboxylic acid product **2** were determined at this stage by ^{1}H NMR analysis using 1,2-dibromoethane as the internal standard. Identity of **2** was confirmed from the purified compound isolated by preparative thin-layer chromatography using a mixed solvent of n-hexane:ethyl acetate:acetic acid (60:40:0.5 *v*/v/v) as an eluent. The ^{1}H NMR spectrum was consistent with the previous report [28,47]. ^{1}H NMR (400 MHz, CD_3OD) δ: 7.93 (2H, d, $J = 8.0$ Hz), 7.74 (1H, t, $J = 8.0$ Hz), 7.65 (2H, t, $J = 8.0$ Hz), 3.47 (2H, t, $J = 8.0$ Hz), 2.55 (2H, t, $J = 8.0$ Hz).

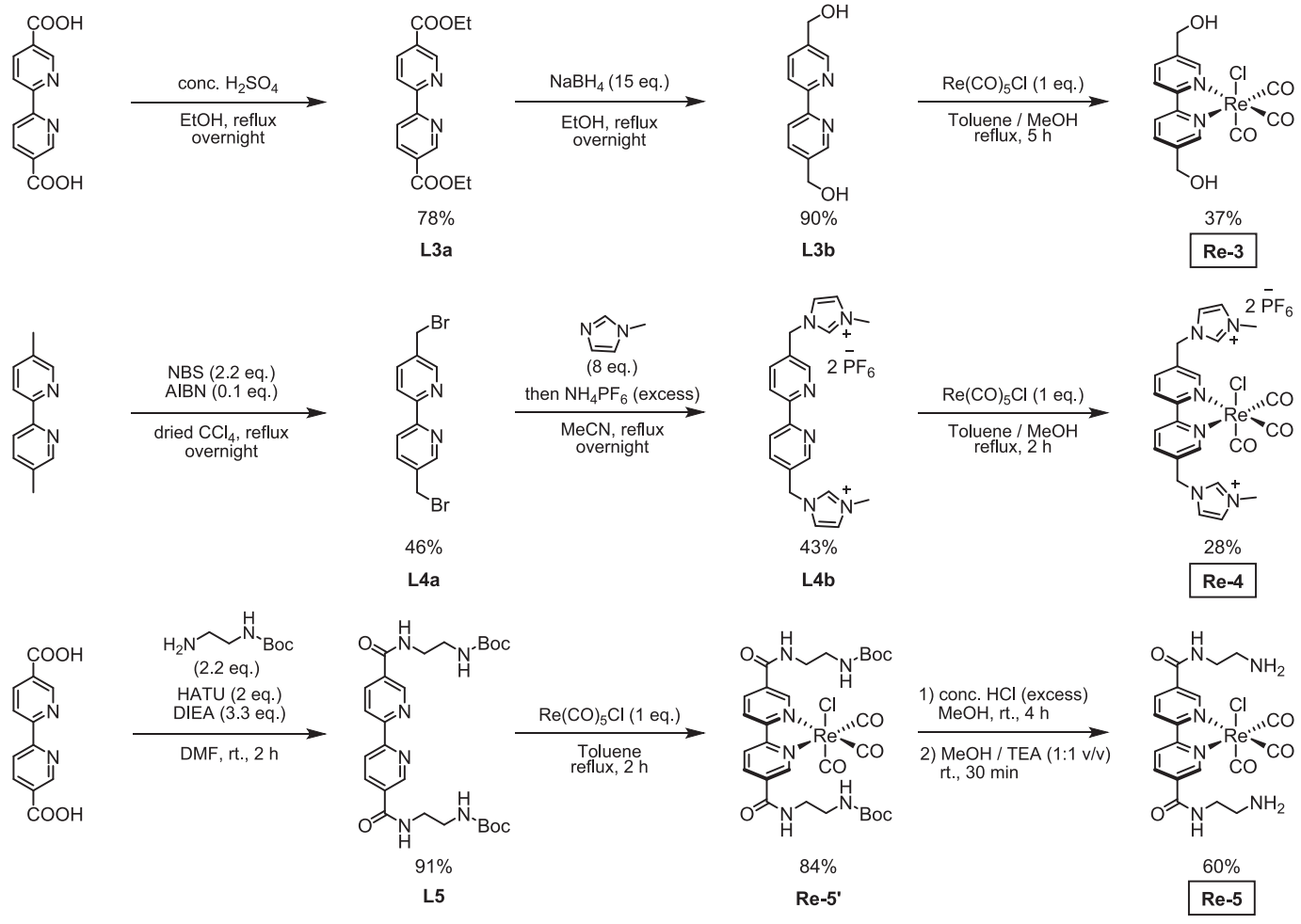

Scheme 1. Synthesis of **Re-3**, **Re-4**, and **Re-5**

For **Re-4**, a slightly modified preparation was used. In detail, a solution of **Re-4** (0.94 mg, 0.001 mmol) in DMSO (1 mL) was first prepared. Then, to this solution was added sodium *tert*-butoxide (0.58 mg, 0.006 mmol), and the mixture was stirred at room temperature for 30 min before **1** (16.8 mg, 0.1 mmol) and BIH (22.4 mg, 0.1 mmol) were added. Next, the vial was sealed with a rubber septum, and the following steps are identical to the aforementioned procedure.

3. Results and discussion

3.1. Synthesis of Re complexes

Each Re complex was prepared according to the previously reported procedure with minor modifications [48]. In a typical synthesis, equimolar amounts of $Re(CO)_5Cl$ and the corresponding bipyridine ligand were heated under reflux in toluene or in a mixed solvent of toluene and methanol under an inert atmosphere. The desired Re complexes gradually precipitated from the reaction mixture as yellow or orange solids and were isolated by filtration and further purified by recrystallization. The identity and purity of each complex were confirmed by NMR spectroscopy, mass spectrometry, elemental analysis, and single-crystal X-ray diffraction analysis.

Complexes **Re-1** and **Re-2** were synthesized from commercially available 2,2′-bipyridine and 2,2′-bipyridine-5,5′-dicarboxylic acid, respectively. In contrast, the bipyridine derivatives for complexes **Re-3** and **Re-4** were obtained through two-step syntheses, as outlined in Scheme 1 and described in detail in the Experimental Section. Ligand **L3b** was prepared by esterification of 2,2′-bipyridine-5,5′-dicarboxylic acid with ethanol, followed by reduction with $NaBH_4$ to afford the corresponding diol. For the synthesis of **L4b**, the methyl groups of 5,5′-dimethyl-2,2′-bipyridine were first brominated using *N*-bromosuccinimide, and the resulting bromomethyl groups (**L4a**) were subsequently substituted with 1-methylimidazole. Final ion exchange with NH_4PF_6 afforded the desired imidazolium-functionalized ligand **L4b**.

For the preparation of the bipyridine derivative for **Re-5**, the first step involved the formation of amide bonds by substitution reaction of the carboxyl groups of 2,2′-bipyridine-5,5′-dicarboxylic acid using mono-protected ethylenediamine. In the subsequent step, we found that performing the Re complexion reaction first to afford the Boc-protected **Re-5′**, followed by deprotection, provided **Re-5** in promising yield and purity. When the deprotection step was carried out prior to the Re complexation, the subsequent complexation reaction led to the formation of insoluble materials and left a substantial amount of unreacted ligand. This behavior is possibly attributed to side reactions caused by the coordination of free amino groups to the Re center. It should be noted that the concentrated hydrochloric acid was used for the deprotection reaction of Boc group, after which the solution was neutralized by triethylamine to afford the free amine groups. The resulting byproduct, triethylamine hydrochloride, was readily removed by washing with a $CHCl_3$-triethylamine solution (100:1 *v*/v). Nevertheless, the chloride salt of **Re-5** was used to grow the diffraction-quality crystals, and it was found that the chloride ions exhibit the intermolecular interactions within the crystal structure (vide infra).

3.2. Characterization of Re complexes

Crystal Structures. The molecular structures of **Re-2** to **Re-5** were elucidated by single-crystal X-ray diffraction analysis. Thermal ellipsoid model of these complexes are shown in Fig. 3, and crystallographic data and refinement details are summarized in Table 1. Similar to the benchmark complex **Re-1** [49], all Re complexes adopt an octahedral coordination geometry and crystallize in the monoclinic lattice system with the $P2_1/c$ space group, containing four formula units per unit cell. Selected bond parameters are shown and compared in Fig. 4 and **Table S1–4**.

For **Re-2**, one Re complex molecule co-crystallizes with one molecule of diethyl ether to form the asymmetric unit (**Fig. S1–2**). Each carboxylic acid group participates in hydrogen bonding, interacting with a carboxyl group of a neighboring **Re-2** molecule on one side and with the oxygen atom of the diethyl ether molecule on the other side. This arrangement generates a solvent–complex–complex–solvent sequence along the *a* axis (**Fig. S3**). It is worth noting that a different crystal form, in which the same Re complex co-crystallizes with methanol in the monoclinic C_2/c space group, has been reported [50]. In that structure, hydrogen bonding exists between the oxygen atom of a carbonyl group and a hydrogen atom on the aromatic ring. In our present structure, the Re—N bond distances are 2.181(3) Å and 2.182(3) Å for Re1–N1 and Re1–N2, respectively, which are in agreement with the previous reported values (2.179(4) Å for both sides) [50] and slightly longer than those of **Re-1** (2.176(5) and 2.173(5) Å).

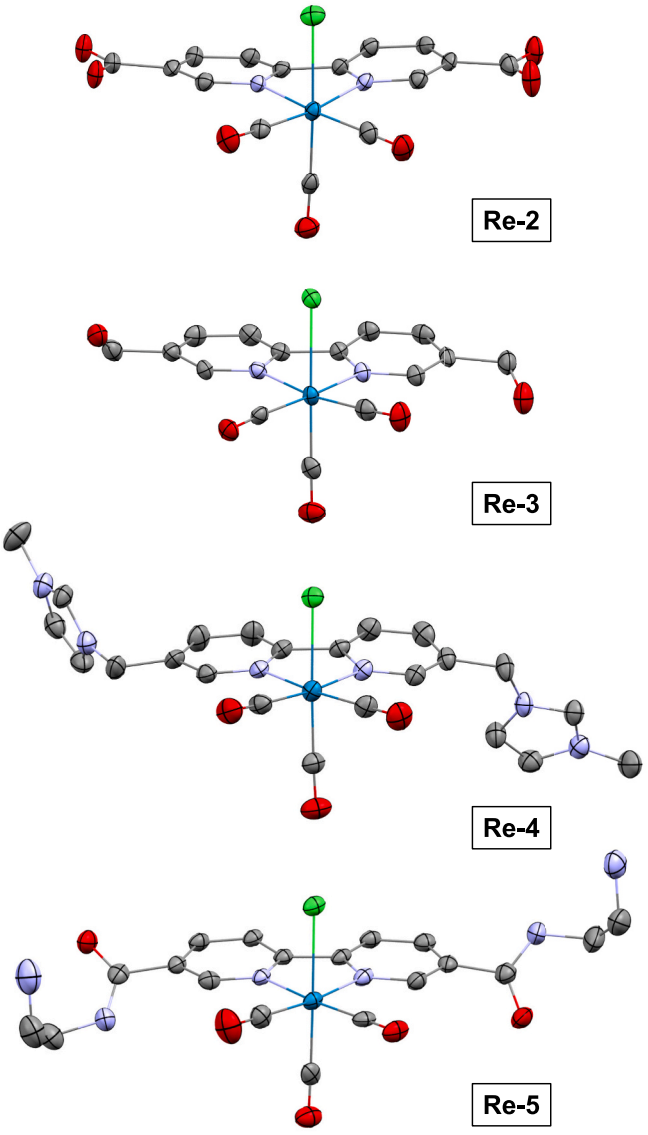

Fig. 3. Thermal ellipsoid model (50% probability level) of **Re-2**, **Re-3**, **Re-4**, and **Re-5**. Hydrogen atoms, counter ions, and co-crystallized solvents are omitted for clarity. Element color: gray = C; purple = N; red = O; green = Cl; blue = Re. (For interpretation of the references to color in this figure legend, the reader is referred to the web version of this article.)

In the crystal structure of **Re-3**, one Re complex molecule and one ethanol molecule constitutes the asymmetric unit (**Fig. S4–5**). Hydrogen bonding between the hydroxy groups of the complex and the ethanol molecule, together with the π-π stacking interactions between bipyridine

Table 1
Crystallographic data and structure refinement for **Re-2**, **Re-3**, **Re-4**, and **Re-5**.

	Re-2	**Re-3**	**Re-4**	**Re-5**[a]
Empirical formula	$C_{19}H_{18}ClN_2O_8Re$	$C_{17}H_{18}ClN_2O_6Re$	$C_{23}H_{22}ClF_{12}N_6O_3P_2Re$	$C_{21}H_{30}Cl_3N_6O_7Re$
Formula weight	624.00	567.98	942.05	771.06
Temperature / K	123.00(10)	122.6(6)	123.01(13)	123.00(10)
Crystal system	monoclinic	monoclinic	monoclinic	monoclinic
Space group	$P2_1/c$	$P2_1/c$	$P2_1/c$	$P2_1/c$
a / Å	13.2795(4)	18.7609(5)	12.4871(5)	19.1388(5)
b / Å	15.0471(4)	11.3124(3)	17.3640(5)	8.94350(10)
c / Å	11.9122(4)	8.9787(2)	14.6200(5)	17.9852(4)
α / °	90	90	90	90
β / °	112.742(4)	93.700(2)	105.752(4)	107.967(2)
γ / °	90	90	90	90
Volume / Å^3	2195.22(13)	1901.58(8)	3050.95(19)	2928.36(11)
Z	4	4	4	4
D_{calc} / g cm^{-3}	1.888	1.984	2.051	1.749
Radiation	Mo K$_\alpha$ (λ = 0.71073 Å)	Mo K$_\alpha$ (λ = 0.71073 Å)	Mo K$_\alpha$ (λ = 0.71073 Å)	Mo K$_\alpha$ (λ = 0.71073 Å)
Reflections collected	22,534	19,843	25,587	29,783
Unique reflections	5938 (R_{int} = 0.0461)	5227 (R_{int} = 0.0477)	8167 (R_{int} = 0.0371)	7881 (R_{int} = 0.0343)
GooF on F^2	1.002	1.063	1.045	1.079
R_1, wR_2 ($I \geq 2\sigma$ (I)]	0.0334, 0.0633	0.0327, 0.0769	0.0374, 0.0786	0.0368, 0.0961
R_1, wR_2 (all data)	0.0563, 0.0685	0.0421, 0.0805	0.0583, 0.0842	0.0518, 0.1017
$\Delta\rho_{max}$, $\Delta\rho_{min}$ / e Å^{-3}	1.56, −1.00	1.60, −0.85	1.59, −0.60	2.01, −1.54

[a] Residual electron/hole peaks were filtered off by Mask option in Olex2.

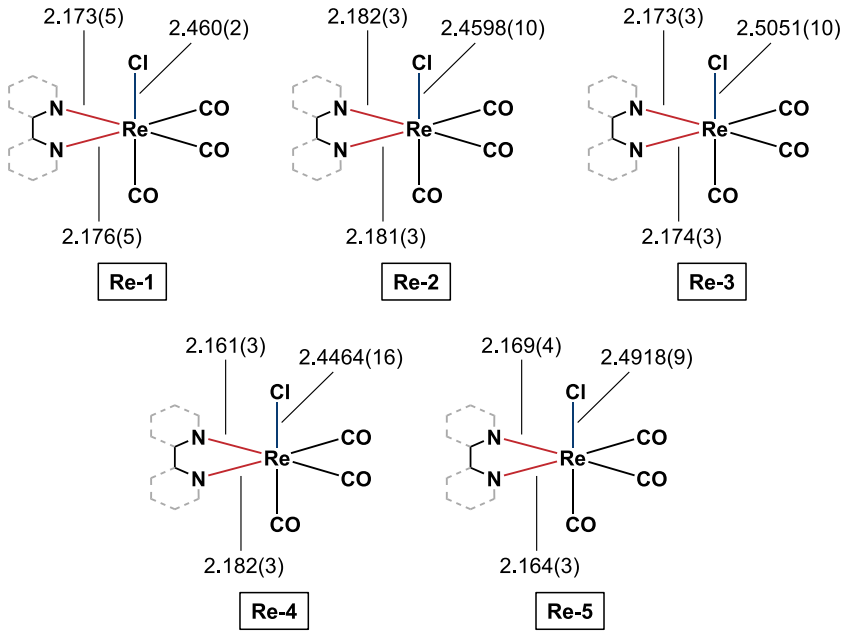

Fig. 4. Comparison of bond distances (Å) in each Re complex.

units, establishes a packing structure that propagates along the c axis (**Fig. S6**). In addition, adjacent **Re-3** molecules along the a axis direction are linked by the O–H···Cl interactions, which leads to an elongation of the Re—Cl bond to 2.5051(10) Å. The Re—N bond distances are 2.174 (3) Å and 2.173(3) Å, which are essentially identical to those of **Re-1**.

The crystal structure of **Re-4** contains one Re complex cation and two PF_6 anions in the asymmetric unit (**Fig. S7–8**). Positional disorder originated from the exchange of the axial chloro ligand and the trans carbonyl ligand was observed and refined over two positions with occupancies of 0.83 and 0.17. The packing structure is stabilized by the C–H···F hydrogen bonding interactions between the PF_6 anions and the hydrogen atoms on the imidazolium groups, similar to that observed in the crystal structure of the ligand **L4** [51], as well as by interactions involving the methylene bridges (**Fig. S9**). The Re—N bond distances of **Re-4** are 2.182(3) Å and 2.161(3) Å for Re1–N1 and Re1–N2, respectively. The significant difference between these values is likely attributable to steric effects of the bulky imidazolium substituents.

Re-5 crystallizes as a chloride salt, in which the asymmetric unit consists of one Re complex cation and two chloride anions (**Fig. S10–11**). Intermolecular interactions in the crystal are dominated by a hydrogen-bonding network involving the oxygen atoms of the carbonyl groups and the hydrogen atoms of both the amide and the terminal amino groups. The axial chloro ligand also participates in hydrogen bonding with a hydrogen atom of an amino group from the inversion-center-generated molecule (**Fig. S12**), resulting in a relatively long Re—Cl bond distance of 2.4920(10) Å). The free chloride anions further contributes the hydrogen-bonding network by bridging neighboring Re complexes through the terminal amino groups. The Re—N bond distances in **Re-5** are relatively short, at 2.169(4) and 2.164(3) Å.

Overall, these crystallographic analyses show that all complexes retain the same classical octahedral Re(I) diimine tricarbonyl core, whereas the introduced functional groups mainly modify the

intermolecular interactions and, in some cases, slightly alter the local coordination environment around the Re center.

UV–visible absorption spectra. The UV–visible absorption spectra of the Re complexes were measured in a degassed DMF solution (40 μM) at room temperature (Fig. 5). All complexes exhibit an intense absorption band in the ultraviolet region, which can be assigned to the bipyridine-based π–π* transition, along with a moderate absorption band in the visible-light region attributed to the singlet metal-to-ligand charge transfer (^{1}MLCT) transition from the Re center to π* orbital of the bipyridine ligand [52,53]. Compared with **Re-1**, clear redshifts were observed for **Re-2**, **Re-4** and **Re-5** in both ^{1}MLCT and π–π* bands. These shifts can be rationalized by the stabilization of the bipyridine-based π* lowest unoccupied molecular orbital resulting from the increased π-acceptor character of the substituted ligands [52]. This electronic effect is consistent with the stronger CO stretching observed in the infrared spectra, which indicates the smaller extent of electron back-donation, and the positive shifts of the reduction potentials obtained from cyclic voltammetry measurements (vide infra).

Photoluminescence measurements revealed that only **Re-1** and **Re-3** exhibit weak emission bands at 572 and 570 nm, respectively, which become detectable only when a wide slit width is used (**Fig. S14**). These emissions originate from the relaxation of the MLCT excited state [53]. It is well known that increasing the electron-withdrawing character of diimine ligands generally shortens the excited-state lifetime and enhances the rate of nonradiative decay [52,54], which accounts for the absence of emission from **Re-2**, **Re-4**, and **Re-5**. Notably, negligible emission was observed from **Re-2** in DMF, whereas a closely related complex bearing a 2,2′-bipyridine-4,4′-dicarboxylic acid ligand was reported to show a weak emission at 600 nm in the same solvent at room temperature [55].

These spectroscopic results indicate that the introduced substituents primarily tune the electronic structure of the bipyridine ligand, leading to systematic changes in the MLCT energy and excited-state properties of the Re complexes.

Infrared spectra. Infrared (IR) spectra were recorded directly from the solid samples using the attenuated total reflectance (ATR) method (Fig. 6 and **S15**). All Re complexes exhibit a sharp and intense band in the range of 2024–2013 cm^{-1}, together with a broad and intense band at 1886–1867 cm^{-1}, both of which originate from the stretching vibrations of CO ligands. While *fac*-tricarbonyl Re complexes typically show three C—O stretching bands in the solution [56–58], it is also reported that broad and unresolved bands are observed in the solid state [59,60].

Moreover, characteristic absorption bands arising from the introduced functional groups can be clearly identified. In the spectrum of **Re-2**, a broad and weak absorption band assignable to the carboxylic acid group appears in the region of 3400–2500 cm^{-1}. The spectrum of **Re-3** shows two distinctive bands at 3633 cm^{-1} and 3390 cm^{-1} attributable to

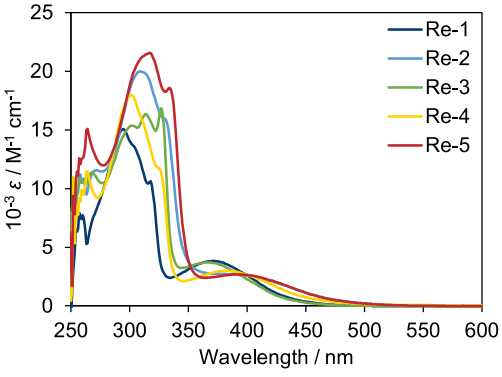

Fig. 5. UV–visible absorption spectra of each Re complex measured at room temperature using DMF as the solvent (40 μM) in a glass cell (1 cm).

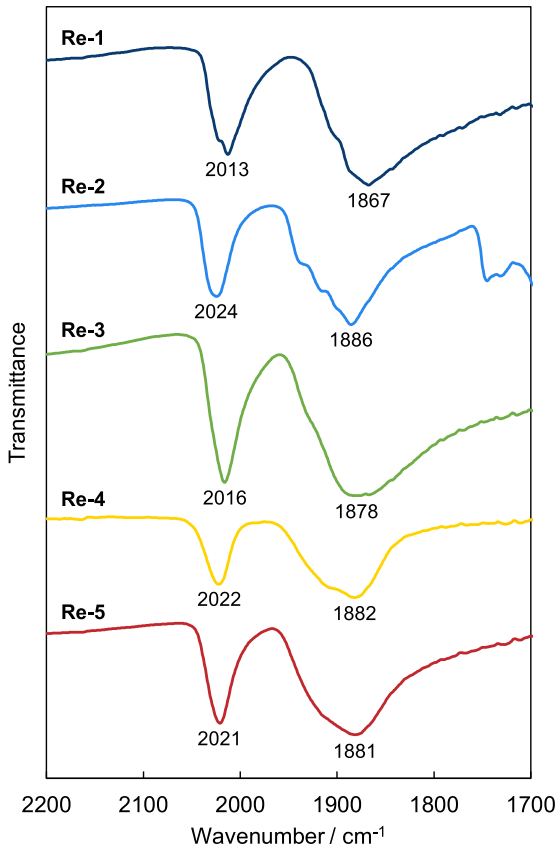

Fig. 6. Infrared spectra of Re complexes measured from solid samples using Attenuated Total Reflectance (ATR) method.

O—H stretching vibration. The unusually sharp appearance of these bands suggests the absence of strong hydrogen bonding in the solid state of the complex. The spectrum of **Re-4** exhibits strong absorptions at 820 cm^{-1} and 743 cm^{-1}, characteristic of the bending mode of the imidazolium ring [61]. For **Re-5**, a broad absorption band in the region of 3700–2100 cm^{-1} is observed, within which a small peak at 3207 cm^{-1} can be assigned to the N—H stretching vibration of primary amine groups. The exceptionally broad nature of this band indicates the presence of extensive intermolecular hydrogen bonding [62].

The electronic effects of the substituents are most clearly reflected in the C—O stretching frequencies (Fig. 6 and Table 2). **Re-1** exhibited the C—O stretching vibration at 2013 and 1867 cm^{-1}. In **Re-3**, these bands shift slightly to higher wavenumbers (2016 and 1878 cm^{-1}). In contrast, **Re-2**, **Re-4**, and **Re-5** how more pronounced shifts to higher frequencies for both the high-frequency (2024–2021 cm^{-1}) and the low-frequency (1886–1881 cm^{-1}) bands. These shifts indicate differences in the extent of π back-donation from the Re center to the CO ligands; a lower electron density at the metal center leads to weaker back-donation, and thus stronger C—O bond, resulting in higher stretching frequencies. Overall, these IR data demonstrate that the introduced functional groups exhibit an electron-withdrawing effect on the Re center, and that this effect is particularly pronounced for **Re-2**, **Re-4**, and **Re-5**.

Electrochemical properties. Cyclic voltammetry (CV) was performed for all Re complexes to gain insight into their electrochemical behaviors. Measurements were conducted under an Ar atmosphere in acetonitrile solutions containing 0.5 mM of the Re complex, and 0.1 M tetrabutylammonium hexafluorophosphate ($TBAPF_6$) as a supporting electrolyte. In the case of **Re-5**, DMF was used as the solvent due to the low solubility of the complex in acetonitrile. The resulting CV curves are shown in Fig. 7. All potentials are reported versus the ferrocene/

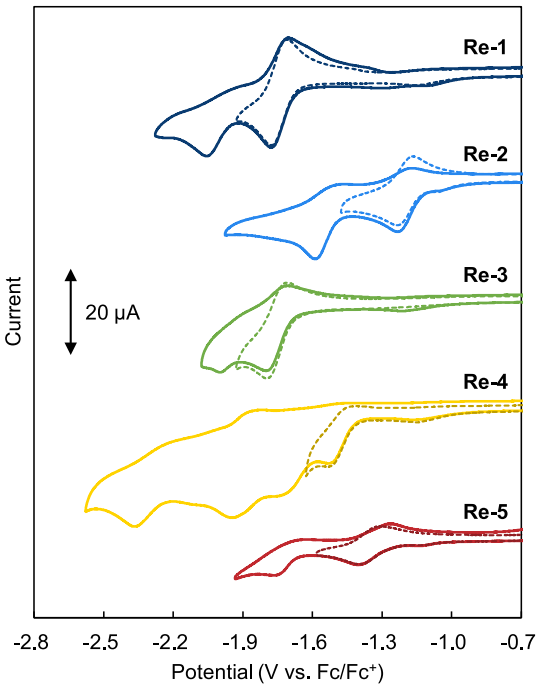

Fig. 7. Cyclic voltammogram of **Re-1** to **Re-4** (0.5 mM) measured in MeCN, and **Re-5** (0.5 mM) measured in DMF. $TBAPF_6$ (0.1 M) was used as a supporting electrolyte for both solvents. The dashed lines represent the curve of the first reduction wave. The measurement was performed under an Ar atmosphere at a scan rate of 100 mV s^{-1} using a glassy carbon (diameter 3 mm) as a working electrode, a Ag/Ag^+ as a reference electrode, and a Pt wire as a counter electrode.

ferrocenium (Fc/Fc^+) redox couple, and the values are summarized in Table 2.

Re-1 shows a reversible wave at −1.73 V and an irreversible wave at −2.05 V, which can be assigned to the reduction of 2,2′-bipyridine ligand and the Re(I) metal center, respectively [63]. By analogy, the first cathodic waves observed for the other Re complexes are also attributed to the reduction of bipyridine moieties, and appear at different potentials depending on the nature of the functional groups [54,55,57]. Notably, the first reduction waves of **Re-2** and **Re-5** are significantly shifted to more positive potentials, as expected for complexes bearing electron-withdrawing groups on the bipyridine ligands. This positive shift, in association with the redshift observed in the UV–visible absorption spectra, can be rationalized by the stabilization of the bipyridine-based π* lowest unoccupied molecular orbital, which in turn lowers the energy gap for MLCT excitation [52,55]. It should be noted that previous reports on electron-donating amino substituents describe a general trend in which such groups shift the reduction wave to more negative potentials [62,64]. This behavior is distinct from the present system, where the installed alkyl amide functionality is electron-withdrawing and therefore consistent with the observed positive shift. Importantly, the first reduction waves exhibit quasi-reversible or reversible behavior, indicating that the one-electron-reduced species are relatively stable under the present conditions. The second reduction peak can be assigned to the reduction of Re(I) center or to the second reduction of the bipyridine ligand, depending on the nature of the installed functional groups. In particular, bipyridine ligands bearing carbonyl groups, such as those in **Re-2** and **Re-5**, are known to accommodate the second additional electron within the ligand resonance structure [65].

The CV behavior of **Re-4** displays a more complicated feature. The first reduction wave is again assigned to the reduction of bipyridine scaffold, and its positive shift relative to that of **Re-1** can be explained by the stabilization of the one-electron-reduced species by the positively charged imidazolium groups [33]. To identify possible reduction processes of the imidazolium groups themselves, the electrochemical behavior of 1,3-dimethylimidazolium iodide was examined as a model compound. However, the first reduction peak was observed at a highly negative potential of −2.7 V (vs. Fc/Fc^+), which lies outside the potential window (**Fig. S16**). Consistent with this observation, previous reports have also shown no cathodic responses for the similar methyl imidazolium groups up to −2.6 V vs. Fc/Fc^+ [35,66]. Therefore, the additional reduction waves of **Re-4** are unlikely to originate from the imidazolium groups, and are more plausibly associated with further reduction of the bipyridine ligand and/or the Re center, although a definitive assignment cannot be made at this stage. These electrochemical results clearly show that the introduced functional groups tune the reduction potentials of the Re complexes by modulating the electronic structure of the bipyridine ligand, which is in good agreement with the results observed in the UV–visible and IR spectroscopic studies.

We further investigated the electrochemical behaviors of the Re complexes under a CO_2 atmosphere, and the corresponding CV curves are overlaid with those measured under Ar in Fig. 8. As shown in Fig. 8,

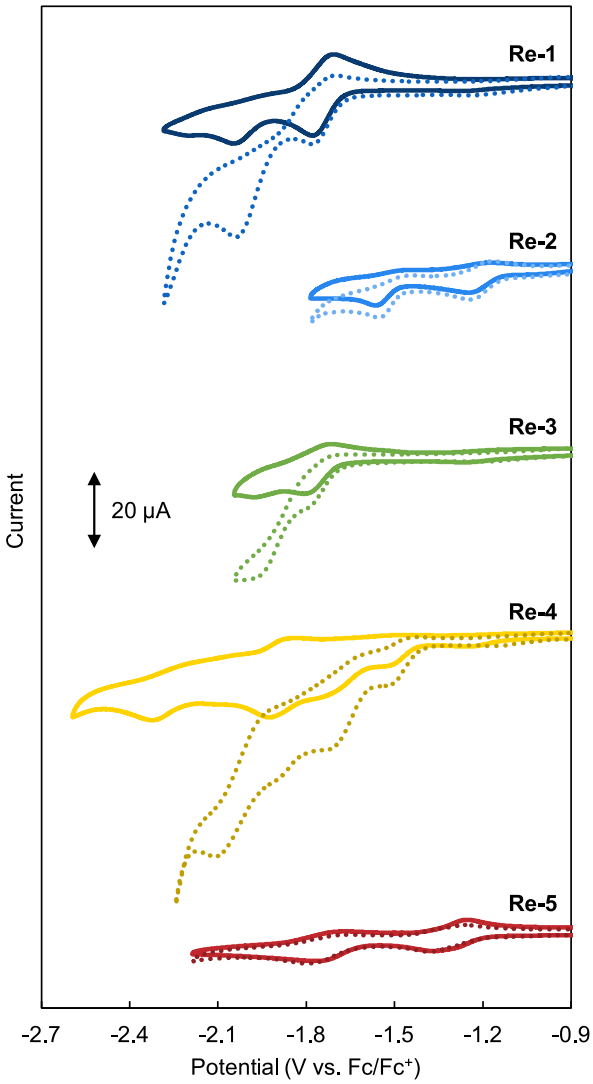

Fig. 8. Cyclic voltammogram of **Re-1** to **Re-4** (0.5 mM) measured in MeCN, and **Re-5** (0.5 mM) measured in DMF, under an Ar (solid lines) and a CO_2 (dashed lines) atmosphere. $TBAPF_6$ (0.1 M) was used as a supporting electrolyte for both solvents. All measurements were performed at a scan rate of 100 mV s^{-1} using a glassy carbon (diameter 3 mm) as a working electrode, a Ag/Ag^+ as a reference electrode, and a Pt wire as a counter electrode.

Table 2
Numerical data from the UV–visible absorption spectra, emission spectra, infrared spectra, and cyclic voltammograms of Re complexes.

Complex	λ_{max} / nm (10^{-3} ε / M^{-1} cm^{-1})		Emission / nm	ν (CO) / cm^{-1}	Reduction[b] (V vs. Fc/Fc^+)
	π–π^* transition	^{1}MLCT transition			
Re-1	294 (15.06) 303 (13.67)[a] 318 (10.61)	371 (3.81)	572	2013, 1867	−1.73 (r) −2.05 (i)
Re-2	309 (19.98) 329 (15.99)[a]	380 (2.72)	n.d.	2024, 1886	−1.23 (i) −1.58 (i)
Re-3	302 (15.37) 313 (16.34) 327 (16.86)	367 (3.70)	570	2016, 1878	−1.79 (i) −1.99 (i)
Re-4	302 (17.97) 325 (11.74)[a]	382 (2.99)	n.d.	2022, 1882	−1.52 (i) −1.74 (i) −1.95 (i) −2.36 (i)
Re-5	317 (21.56) 334 (18.59)	392 (2.68)	n.d.	2021, 1881	−1.33 (r) −1.76 (i)

i = irreversible (peak potential value is reported). n.d. = no detection.
[a] Absorption shoulder.
[b] r = reversible.

Re-1, **Re-3**, and **Re-4** exhibit significant current enhancements at the second reduction wave compared to the measurements under an Ar atmosphere. These results indicate appreciable interactions between CO_2 and the two-electron-reduced forms of these complexes. In contrast, **Re-2** exhibits only a minor current enhancement, and **Re-5** displays nearly identical CV curves under Ar and CO_2 atmospheres, suggesting negligible interaction with CO_2.

3.3. Photocatalytic study

Photocatalytic CO_2 reduction. We first evaluated the catalytic activities of the Re complexes in the photocatalytic reduction of CO_2 under visible-light irradiation. In a typical experiment, the reaction was conducted using 0.5 mM of the Re complex in a mixed solvent of DMF and triethanolamine (TEOA) (5:1 *v*/v), with BIH as a sacrificial electron donor and the Xenon-arc lamp (300 W, ≥420 nm) as the light source for 3 h. The results are summarized in Fig. 9. In the case of **Re-4**, sodium *tert*-butoxide was additionally added to the reaction mixture to deprotonate the imidazolium groups and generate the corresponding carbene species in situ. Analysis of the gaseous products revealed that CO was the main product for all Re complexes, accompanied by only trace amounts of hydrogen (turnover number (TON) <1). Compared with the benchmark catalyst **Re-1**, the functionalized derivatives showed comparable or, in most cases, inferior activities for CO production. In particular, no detectable CO formation was observed when **Re-5** was used as the catalyst. The origin of these differences in catalytic performance will be discussed in detail in conjunction with the electrochemical properties of each complex in the *Discussion* section (vide infra).

Photocatalytic carboxylation of 1 with CO_2. In our previous work, we demonstrated that **Re-1** efficiently catalyzes the visible-light-driven carboxylation of **1** with CO_2, affording the corresponding carboxylic acid **2** with a high turnover number and excellent regioselectivity [28]. In the present study, we extended this reaction to a series of functionalized Re complexes and compared their catalytic performances with that of the benchmark **Re-1**.

In a typical experiment, the reaction was conducted in a DMSO solution of **1** containing the Re complex as the catalyst with BIH as the sacrificial electron donor, under the irradiation with a blue LED (465–470 nm) for 16 h at room temperature. The results are summarized in Table 3. Under these conditions, all Re complexes afforded similar yields of product **2**, with turnover numbers in the range of 20–24, indicating that the catalytic activity for the carboxylation reaction is essentially independent of the installed functional groups. This behavior is in sharp contrast to the photocatalytic CO_2 reduction, in which the electronic properties exert a pronounced influence on catalytic performance. In the present carboxylation reaction, however, comparable activities are observed for all complexes despite their substantially different electronic properties. It is also noteworthy that only trace amount of CO (TON <1) were detected in all experiments, consistent with our previous study, confirming that the CO_2 reduction pathway is effectively suppressed under these conditions.

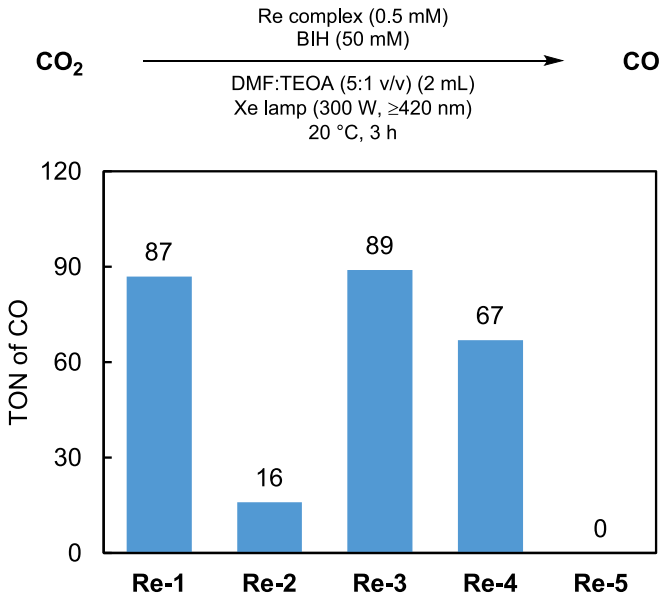

Fig. 9. Formation of CO from photocatalytic reduction of CO_2 by Re complexes. The reaction was conducted in a glass vial containing Re complex (0.5 mM) and BIH (50 mM) dissolved in a mixture of DMF:TEOA (5:1 v/v) (2 mL). The solution was saturated with CO_2 (1 atm) for 20 min then irradiated by a Xe lamp (300 W, ≥420 nm) for 3 h during which the temperature was maintained at 20 °C. At the end of the reaction, gaseous products were analyzed by gas chromatography. When **Re-4** was used, sodium *tert*-butoxide was also added to the reaction mixture.

Analysis of the crude reaction mixture revealed the [2 + 2] dimerization product (**3**) as the major side product (TON = 28–32), and the hydroacylation product (**4**) as a minor side product (TON = 3–5). The product **4** was generated from the coupling reaction between **1** and the BI radical formed via one-electron oxidation of BIH followed by deprotonation, as previously reported by our group (for the details, see **Fig. S17**) [67]. On the other hand, the detailed mechanism for the dimerization reaction, which rapidly consumes the starting material **1** and thus represents a major undesired side reaction, remains unclear (For the hypothetical mechanism for the generation of **3**, see P·S18 in the SI). Elucidating and suppressing this dimerization pathway will be the key to further improving the efficiency of this catalytic system.

4. Discussion

To rationalize the different catalytic performances observed in photocatalytic CO_2 reduction, we further considered the electrochemical behaviors of the Re complexes under a CO_2 atmosphere by cyclic voltammetry. As described in Fig. 8, **Re-1**, **Re-3**, and **Re-4** exhibit significant current enhancements, particularly at the second reduction

Table 3
Product distribution from photocatalytic carboxylation of **1** with CO_2 by Re complexes.[a]

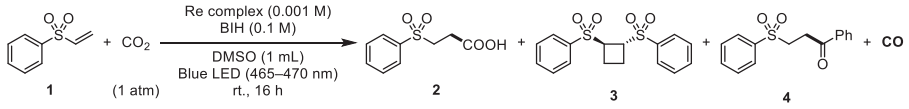

Entry	Catalyst	TON of Products			
		2[b]	**3**[b]	**4**[b]	**CO**
1	**Re-1**	23	28	4	<1
2	**Re-2**	21	29	3	<1
3	**Re-3**	24	29	4	<1
4	**Re-4**	20	28	5	<1
5	**Re-5**	21	32	4	<1

[a] The reaction was conducted in a glass vial containing **1** (0.1 M), Re complex (0.001 M), and BIH (0.1 M) dissolved in DMSO (1 mL). The solution was saturated with CO_2 (1 atm) for 15 min then irradiated by a Blue LED (465–470 nm) for 16 h under room temperature. When **Re-4** was used, sodium *tert*-butoxide (0.006 M) was also added to the reaction mixture.

[b] TON was calculated based on crude ^{1}H NMR using 1,2-dibromoethane as the internal standard.

wave, whereas **Re-2** and **Re-5** show negligible changes. These results, together with the photocatalytic experiments, indicate a correlation between the reduction potentials and the catalytic activities in CO_2 photoreduction. In particular, the poor catalytic performance of **Re-2** and **Re-5** can be attributed to the decreased nucleophilicity of the Re center by coordination to strongly electron-withdrawing ligands. This interpretation is consistent with previous reports, which showed that bipyridine derivatives bearing carbonyl groups can accommodate and stabilize electrons within the conjugated ligands, thereby suppressing reduction of Re(I) to the catalytically active Re(0) species that reacts with CO_2 [65]. The present catalytic behavior can be qualitatively compared with that of natural metalloenzymes such as [NiFe] carbon monoxide dehydrogenase (CODH). In both systems, CO_2 activation involves interaction of the substrate carbon atom with an electron-rich metal center. However, [NiFe] CODH operates with a higher degree of mechanistic sophistication: the active-site geometry is precisely organized, nearby residues and metal centers cooperatively stabilize bound intermediates and facilitate proton transfer, and electron delivery is efficiently mediated through the protein framework. While the present Re complexes rely primarily on the electronic properties of the ligand framework and the metal center, the enzymatic system benefits from cooperative substrate binding, secondary coordination sphere interactions, and controlled proton/electron transfer pathways. These features enable highly efficient and selective CO_2 conversion under mild conditions.

Bridging between natural enzymes and molecular systems, artificial metalloenzymes have demonstrated that incorporation of molecular catalysts into protein scaffolds can enhance catalytic performance by introducing elements of structural and environmental control. In such systems, improvements in catalytic activity and product selectivity have been attributed to factors such as regulation of the local environment around the metal centers [68,69], the modulation of the coordination geometry [70], and the availability of the redox-active species within the protein framework [70,71]. In contrast, the present molecular systems do not incorporate such levels of structural and environmental control, which likely contributes to their more limited catalytic performance. Taken together, these comparisons highlight that, beyond electronic tuning, the integration of secondary coordination sphere effects and controlled reaction environments is a key factor for achieving higher catalytic efficiency and selectivity in CO_2 conversion systems.

Collectively, the present results demonstrate that the electronic effects of the ligand functional groups impact the photocatalytic activity of Re complexes for CO_2 reduction. In contrast, in the carboxylation reaction of alkenes, comparable activities are observed for all complexes despite their substantially different electronic properties. This difference indicates that the role of ligand electronic effects differs depending on the type of CO_2 utilization. At present, there is no direct experimental evidence to fully rationalize this behavior; however, in contrast to CO_2 reduction, the carboxylation reaction may proceed through a different reaction pathway in which the rate-determining step is less sensitive to the electronic properties of the catalyst. As a result, variations in ligand functionality have a limited influence on the overall catalytic performance under the present conditions. In line with this consideration, ^{1}H NMR measurements of **Re-5** under a CO_2 atmosphere revealed slight variations in peak splitting patterns, suggesting the presence of weak interactions between CO_2 and the functional groups (**Fig. S20**). These observations indicate that such interactions, if present, are relatively weak under the present conditions, and a more detailed investigation of in situ speciation remains an important subject for future study.

The present study provides a useful set of experimental data that clarifies both the potential and the limitations of simple ligand functionalization on the Re(I) diimine complex platform. In the current series, the electronic effects of the substituents appear to dominate the observed reactivity, while the introduction of additional functional groups does not yet lead to clear improvements in catalytic performance. These results suggest that future designs might benefit from more refined ways of separating electronic tuning from other structural modifications, such as modifying substituent positions or introducing electronically more neutral linker groups. Such strategies are expected to provide a more suitable basis for systematically evaluating how different types of ligand modifications influence reactivity in Re-based systems and for guiding the development of improved molecular catalysts for sustainable chemical transformations.

5. Conclusions

In this work, we have designed, synthesized, and systematically studied a series of Re bipyridine tricarbonyl complexes. All new complexes were fully characterized by single-crystal X-ray diffraction analysis, as well as by spectroscopic and electrochemical methods, which allowed us to correlate their molecular properties with the electronic effects introduced by ligand substitution. Complexes bearing electron-withdrawing substituents (**Re-2**, **Re-4**, and **Re-5**) exhibit clear red-shifts in their absorption spectra, higher C—O stretching frequencies, and more positive reduction potentials, indicating stabilization of the bipyridine π^* orbitals and decreased electron density at the Re center. These electronic effects have a pronounced impact on photocatalytic CO_2 reduction: in contrast to **Re-1**, these derivatives show inferior or negligible activity for CO formation, which can be attributed to a reduced ability of the Re center to accumulate electron density and activate CO_2. In contrast, all complexes display comparable catalytic performance in the visible-light-driven carboxylation of **1** with CO_2,

indicating that ligand electronic effects, while critical for CO_2 reduction, play a much less decisive role in this carboxylation reaction within the present complexes.

Overall, this study provides a systematic experimental picture of how ligand modification influences the properties and reactivity of Re(I) bipyridine tricarbonyl complexes, and shows that different CO_2 utilization reactions can respond quite differently to the same structural changes. The present work provides a useful reference point for future studies, and these insights will help guide the design to improve Re-based molecular catalysts for CO_2 utilization. Detailed mechanistic studies, design and synthesis of new Re complex derivatives and further improvements on catalytic performance are currently underway in our laboratory.

CRediT authorship contribution statement

Phurinat Lorwongkamol: Writing – review & editing, Writing – original draft, Validation, Methodology, Investigation, Data curation, Conceptualization. **Yutaka Saga:** Writing – review & editing, Writing – original draft, Project administration, Methodology, Funding acquisition, Conceptualization. **Tetsuya Kambe:** Validation, Methodology, Funding acquisition. **Mio Kondo:** Validation, Methodology, Funding acquisition. **Shigeyuki Masaoka:** Writing – review & editing, Supervision, Project administration, Funding acquisition, Conceptualization.

Declaration of competing interest

The authors declare no competing interest.

Acknowledgements

This work was supported by the Japan Society for the Promotion of Science KAKENHI [Grant Nos. 22K21348, 23H04903 (Green Catalysis Science), and 24H00464 (S.M.); 22K06525 and 25K22528 (Y.S.); 22H04507, 23H02043, and 25H01671 (T.K.); 22K19086, 23H04628, 24H02212 (Chemical Structure Reprogramming (SReP)), and 25H00885 (M.K.)], Japan Science and Technology Agency (JST) CREST [Grant No. JPMJCR20B6 (S.M.)] and JST FOREST [Grant No. JPMJFR223I (T.K.) and Grant Nos. JPMJFR221S (M.K.)]. Funding was received from the Fujimori Science and Technology Foundation (Y.S.), Kato Foundation for Promotion of Science (KJ-3413) (T.K.), ENEOS Hydrogen Trust Fund (M.K.), and the Mitsubishi Foundation (M.K.). This work used the research equipment shared in the MEXT Project for promoting public utilization of advanced research infrastructure (Program for Supporting Construction of Core Facilities) Grant Number [JPMXS0441200025].

Appendix A. Supplementary data

Supplementary data to this article can be found online at https://doi.org/10.1016/j.jinorgbio.2026.113344.

Data availability

The data supporting this article are included in the supporting information. Crystallographic data have been deposited with Cambridge Crystallographic Data Centre (CCDC): Deposition number: 2525046 (**Re-2**), 2525043 (**Re-3**), 2525045 (**Re-4**), 2525044 (**Re-5**), and 2,526,247 (**3**).

References

[1] A.M. Appel, J.E. Bercaw, A.B. Bocarsly, H. Dobbek, D.L. DuBois, M. Dupuis, J. G. Ferry, E. Fujita, R. Hille, P.J.A. Kenis, C.A. Kerfeld, R.H. Morris, C.H.F. Peden, A. R. Portis, S.W. Ragsdale, T.B. Rauchfuss, J.N.H. Reek, L.C. Seefeldt, R.K. Thauer, G. L. Waldrop, Frontiers, opportunities, and challenges in biochemical and chemical catalysis of CO_2 fixation, Chem. Rev. 113 (2013) 6621–6658, https://doi.org/10.1021/cr300463y.

[2] J.-H. Jeoung, H. Dobbek, Carbon dioxide activation at the Ni,Fe-Cluster of anaerobic carbon monoxide dehydrogenase, Science 318 (2007) 1461–1464, https://doi.org/10.1126/science.1148481.

[3] S.W. Ragsdale, Nickel and the carbon cycle, J. Inorg. Biochem. 101 (2007) 1657–1666, https://doi.org/10.1016/j.jinorgbio.2007.07.014.

[4] Y. Basak, C. Lorent, J.-H. Jeoung, I. Zebger, H. Dobbek, Metalloradical-driven enzymatic CO_2 reduction by a dynamic Ni–Fe cluster, Nat. Catal. 8 (2025) 794–803, https://doi.org/10.1038/s41929-025-01388-5.

[5] T. Hartmann, N. Schwanhold, S. Leimkühler, Assembly and catalysis of molybdenum or tungsten-containing formate dehydrogenases from bacteria, Biochimica et Biophysica Acta (BBA) - Proteins and Proteomics 1854 (2015) 1090–1100, https://doi.org/10.1016/j.bbapap.2014.12.006.

[6] H. Dobbek, Structural aspects of mononuclear Mo/W-enzymes, Coord. Chem. Rev. 255 (2011) 1104–1116, https://doi.org/10.1016/j.ccr.2010.11.017.

[7] M.W. Drover, A guide to secondary coordination sphere editing, Chem. Soc. Rev. 51 (2022) 1861–1880, https://doi.org/10.1039/D2CS00022A.

[8] K.A. Jesse, J.S. Anderson, Leveraging ligand-based proton and electron transfer for aerobic reactivity and catalysis, Chem. Sci. 15 (2024) 16409–16423, https://doi.org/10.1039/D4SC03896G.

[9] J. Hawecker, J.-M. Lehn, R. Ziessel, Efficient photochemical reduction of CO_2 to CO by visible light irradiation of systems containing $Re(bipy)(CO)_3X$ or $Ru(bipy)_3^{2+}$–Co^{2+} combinations as homogeneous catalysts, J. Chem. Soc. Chem. Commun. (1983) 536–538, https://doi.org/10.1039/C39830000536.

[10] A.M. Cancelliere, F. Puntoriero, S. Serroni, S. Campagna, Y. Tamaki, D. Saito, O. Ishitani, Efficient trinuclear Ru(II)–Re(I) supramolecular photocatalysts for CO_2 reduction based on a new tris-chelating bridging ligand built around a central aromatic ring, Chem. Sci. 11 (2020) 1556–1563, https://doi.org/10.1039/C9SC04532E.

[11] K.-H. Chen, N. Wang, Z.-W. Yang, S.-M. Xia, L.-N. He, Tuning of ionic second coordination sphere in evolved rhenium catalyst for efficient visible-light-driven CO_2 reduction, ChemSusChem 13 (2020) 6284–6289, https://doi.org/10.1002/cssc.202000698.

[12] X. Feng, Y. Pi, Y. Song, C. Brzezinski, Z. Xu, Z. Li, W. Lin, Metal–organic frameworks significantly enhance photocatalytic hydrogen evolution and CO_2 reduction with Earth-abundant copper photosensitizers, J. Am. Chem. Soc. 142 (2020) 690–695, https://doi.org/10.1021/jacs.9b12229.

[13] Z. Fu, X. Wang, A.M. Gardner, X. Wang, S.Y. Chong, G. Neri, A.J. Cowan, L. Liu, X. Li, A. Vogel, R. Clowes, M. Bilton, L. Chen, R.S. Sprick, A.I. Cooper, A stable covalent organic framework for photocatalytic carbon dioxide reduction, Chem. Sci. 11 (2020) 543–550, https://doi.org/10.1039/C9SC03800K.

[14] L.-Q. Qiu, K.-H. Chen, Z.-W. Yang, L.-N. He, A rhenium catalyst with bifunctional pyrene groups boosts natural light-driven CO_2 reduction, Green Chem. 22 (2020) 8614–8622, https://doi.org/10.1039/D0GC03111A.

[15] D. Saito, Y. Yamazaki, Y. Tamaki, O. Ishitani, Photocatalysis of a Dinuclear Ru(II)–Re(I) complex for CO_2 reduction on a solid surface, J. Am. Chem. Soc. 142 (2020) 19249–19258, https://doi.org/10.1021/jacs.0c09170.

[16] K. Kamogawa, Y. Shimoda, K. Miyata, K. Onda, Y. Yamazaki, Y. Tamaki, O. Ishitani, Mechanistic study of photocatalytic CO_2 reduction using a Ru(II)–Re(I) supramolecular photocatalyst, Chem. Sci. 12 (2021) 9682–9693, https://doi.org/10.1039/D1SC02213J.

[17] L.-Q. Qiu, K.-H. Chen, Z.-W. Yang, F.-Y. Ren, L.-N. He, Prolonging the triplet state lifetimes of rhenium complexes with imidazole-pyridine framework for efficient CO_2 photoreduction, Chem. A Eur. J. 27 (2021) 15536–15544, https://doi.org/10.1002/chem.202102837.

[18] P.M. Stanley, J. Haimerl, C. Thomas, A. Urstoeger, M. Schuster, N.B. Shustova, A. Casini, B. Rieger, J. Warnan, R.A. Fischer, Host–guest interactions in a metal–organic framework isoreticular series for molecular photocatalytic CO_2 reduction, Angew. Chem. Int. Ed. 60 (2021) 17854–17860, https://doi.org/10.1002/anie.202102729.

[19] P.M. Stanley, C. Thomas, E. Thyrhaug, A. Urstoeger, M. Schuster, J. Hauer, B. Rieger, J. Warnan, R.A. Fischer, Entrapped molecular photocatalyst and photosensitizer in metal–organic framework nanoreactors for enhanced solar CO_2 reduction, ACS Catal. 11 (2021) 871–882, https://doi.org/10.1021/acscatal.0c04673.

[20] J.D.B. Koenig, W.E. Piers, G.C. Welch, Promoting photocatalytic CO_2 reduction through facile electronic modification of N-annulated perylene diimide rhenium bipyridine dyads, Chem. Sci. 13 (2022) 1049–1059, https://doi.org/10.1039/D1SC05465A.

[21] Q. Pan, M. Abdellah, Y. Cao, W. Lin, Y. Liu, J. Meng, Q. Zhou, Q. Zhao, X. Yan, Z. Li, H. Cui, H. Cao, W. Fang, D.A. Tanner, M. Abdel-Hafiez, Y. Zhou, T. Pullerits, S.E. Canton, H. Xu, K. Zheng, Ultrafast charge transfer dynamics in 2D covalent organic frameworks/Re-complex hybrid photocatalyst, Nat. Commun. 13 (2022) 845, https://doi.org/10.1038/s41467-022-28409-2.

[22] L.-Q. Qiu, Z.-W. Yang, X. Yao, X.-Y. Li, L.-N. He, Highly robust rhenium(I) bipyridyl complexes containing dipyrromethene-BF_2 chromophores for visible light-driven CO_2 reduction, ChemSusChem 15 (2022) e202200337, https://doi.org/10.1002/cssc.202200337.

[23] F.-Y. Ren, K. Chen, L.-Q. Qiu, J.-M. Chen, D.J. Darensbourg, L.-N. He, Amphiphilic polycarbonate micellar rhenium catalysts for efficient photocatalytic CO_2 reduction in aqueous media, Angew. Chem. Int. Ed. 61 (2022) e202200751, https://doi.org/10.1002/anie.202200751.

[24] W. Boonta, W. Sangkhun, C. Suppaso, N. Chantanop, W. Panchan, K. Chainok, P. Thamyongkit, T. Sudyoadsuk, K. Maeda, T. Butburee, J. Unruangsri, Rhenium(I) complex-containing amphiphilic metallopolymer stabilizing CdS quantum dots for

synergistically boosting photoreduction of CO_2, ACS Catal. 13 (2023) 12391–12402, https://doi.org/10.1021/acscatal.3c01979.
[25] Y. Kuramochi, Y. Suzuki, S. Asai, T. Suzuki, H. Iwama, M.S. Asano, A. Satake, Significance of the connecting position between Zn(II) porphyrin and Re(I) bipyridine tricarbonyl complex units in dyads for room-temperature phosphorescence and photocatalytic CO_2 reduction: unexpected enhancement by triethanolamine in catalytic activity, Chem. Sci. 14 (2023) 8743–8765, https://doi.org/10.1039/D3SC02430J.
[26] K. Kamogawa, Y. Kato, Y. Tamaki, T. Noguchi, K. Nozaki, T. Nakagawa, O. Ishitani, Overall reaction mechanism of photocatalytic CO_2 reduction on a Re(I)-complex catalyst unit of a Ru(II)-Re(I) supramolecular photocatalyst, Chem. Sci. 15 (2024) 2074–2088, https://doi.org/10.1039/D3SC06059D.
[27] Z. Wang, L. Rotundo, M.Z. Ertem, D.E. Polyansky, G.F. Manbeck, Efficient self-sensitized photochemical CO_2 reduction using $[Re(bpy^{2+})(CO)_3(I)]^{2+}$ and $[Re(bpy^{2+})(CO)_3(CH_3CN)]^{3+}$ photocatalysts with pendent ammonium cations, J. Am. Chem. Soc. 147 (2025) 18796–18813, https://doi.org/10.1021/jacs.5c02523.
[28] P. Lorwongkamol, T. Watanabe, M. Kitada, Y. Uetake, Y. Saga, T. Kambe, M. Kondo, S. Masaoka, *fac*-Re(2,2′-bipyridine)$(CO)_3$Cl catalyzes visible-light-driven functionalization of an organic substrate with CO_2, JACS Au 5 (2025) 4170–4177, https://doi.org/10.1021/jacsau.5c00665.
[29] C. Costentin, G. Passard, M. Robert, J.-M. Savéant, Pendant acid–base groups in molecular catalysts: H-Bond promoters or proton relays? Mechanisms of the conversion of CO_2 to CO by electrogenerated Iron(0)Porphyrins bearing prepositioned phenol functionalities, J. Am. Chem. Soc. 136 (2014) 11821–11829, https://doi.org/10.1021/ja506193v.
[30] E. Haviv, D. Azaiza-Dabbah, R. Carmieli, L. Avram, J.M.L. Martin, R. Neumann, A thiourea tether in the second coordination sphere as a binding site for CO_2 and a proton donor promotes the electrochemical reduction of CO_2 to CO catalyzed by a rhenium bipyridine-type complex, J. Am. Chem. Soc. 140 (2018) 12451–12456, https://doi.org/10.1021/jacs.8b05658.
[31] L. Rotundo, S. Ahmad, C. Cappuccino, D.E. Polyansky, M.Z. Ertem, G.F. Manbeck, A dicationic *fac*-Re(bpy)$(CO)_3$Cl for CO_2 electroreduction at a reduced overpotential, Inorg. Chem. 62 (2023) 7877–7889, https://doi.org/10.1021/acs.inorgchem.3c00624.
[32] L. Rotundo, S. Ahmad, C. Cappuccino, A.J. Pearce, H. Nedzbala, S.R. Bottum, J. M. Mayer, J.F. Cahoon, D.C. Grills, M.Z. Ertem, G.F. Manbeck, Fast catalysis at low overpotential: designing efficient dicationic $Re(bpy^{2+})(CO)_3I$ electrocatalysts for CO_2 reduction, J. Am. Chem. Soc. 146 (2024) 24742–24747, https://doi.org/10.1021/jacs.4c08084.
[33] S. Sung, D. Kumar, M. Gil-Sepulcre, M. Nippe, Electrocatalytic CO_2 reduction by imidazolium-functionalized molecular catalysts, J. Am. Chem. Soc. 139 (2017) 13993–13996, https://doi.org/10.1021/jacs.7b07709.
[34] A. Khadhraoui, P. Gotico, B. Boitrel, W. Leibl, Z. Halime, A. Aukauloo, Local ionic liquid environment at a modified iron porphyrin catalyst enhances the electrocatalytic performance of CO_2 to CO reduction in water, Chem. Commun. 54 (2018) 11630–11633, https://doi.org/10.1039/C8CC06475J.
[35] M.R. Narouz, P. De La Torre, L. An, C.J. Chang, Multifunctional charge and hydrogen-bond effects of second-sphere imidazolium pendants promote capture and electrochemical reduction of CO_2 in water catalyzed by Iron porphyrins, Angew. Chem. Int. Ed. 61 (2022) e202207666, https://doi.org/10.1002/anie.202207666.
[36] S. Sung, X. Li, L.M. Wolf, J.R. Meeder, N.S. Bhuvanesh, K.A. Grice, J.A. Panetier, M. Nippe, Synergistic effects of imidazolium-functionalization on *fac*-Mn$(CO)_3$ bipyridine catalyst platforms for electrocatalytic carbon dioxide reduction, J. Am. Chem. Soc. 141 (2019) 6569–6582, https://doi.org/10.1021/jacs.8b13657.
[37] M.H. Rønne, D. Cho, M.R. Madsen, J.B. Jakobsen, S. Eom, É. Escoudé, H.C. D. Hammershøj, D.U. Nielsen, S.U. Pedersen, M.-H. Baik, T. Skrydstrup, K. Daasbjerg, Ligand-controlled product selectivity in electrochemical carbon dioxide reduction using manganese bipyridine catalysts, J. Am. Chem. Soc. 142 (2020) 4265–4275, https://doi.org/10.1021/jacs.9b11806.
[38] V. Blasczak, A. Murphy, L. Suntrup, K.T. Ngo, B. Reed, S. Groysman, D.C. Grills, J. Rochford, Structure activity relationships for second-coordination sphere functional group dependent CO_2 reduction by manganese bipyridyl electrocatalysts, ChemCatChem 16 (2024) e202301388, https://doi.org/10.1002/cctc.202301388.
[39] I. Azcarate, C. Costentin, M. Robert, J.-M. Savéant, Through-space charge interaction substituent effects in molecular catalysis leading to the design of the most efficient catalyst of CO_2-to-CO electrochemical conversion, J. Am. Chem. Soc. 138 (2016) 16639–16644, https://doi.org/10.1021/jacs.6b07014.
[40] Y. Yamazaki, M. Miyaji, O. Ishitani, Utilization of low-concentration CO_2 with molecular catalysts assisted by CO_2-capturing ability of catalysts, additives, or reaction media, J. Am. Chem. Soc. 144 (2022) 6640–6660, https://doi.org/10.1021/jacs.2c02245.
[41] L. Gu, Y. Zhang, Unexpected CO_2 splitting reactions to form CO with N-heterocyclic carbenes as organocatalysts and aromatic aldehydes as oxygen acceptors, J. Am. Chem. Soc. 132 (2010) 914–915, https://doi.org/10.1021/ja909038t.
[42] E.D. Bates, R.D. Mayton, I. Ntai, J.H. Davis, CO_2 capture by a task-specific ionic liquid, J. Am. Chem. Soc. 124 (2002) 926–927, https://doi.org/10.1021/ja017593d.
[43] C.-H. Yu, C.-H. Huang, C.-S. Tan, A review of CO_2 capture by absorption and adsorption, Aerosol Air Qual. Res. 12 (2012) 745–769, https://doi.org/10.4209/aaqr.2012.05.0132.
[44] V. Ganesan, D. Sivanesan, S. Yoon, Correlation between the structure and catalytic activity of [Cp*Rh(substituted bipyridine)] complexes for NADH regeneration, Inorg. Chem. 56 (2017) 1366–1374, https://doi.org/10.1021/acs.inorgchem.6b02474.
[45] K.P. Divya, S. Sreejith, P. Ashokkumar, K. Yuzhan, Q. Peng, S.K. Maji, Y. Tong, H. Yu, Y. Zhao, P. Ramamurthy, A. Ajayaghosh, A ratiometric fluorescent molecular probe with enhanced two-photon response upon Zn^{2+} binding for in vitro and in vivo bioimaging, Chem. Sci. 5 (2014) 3469–3474, https://doi.org/10.1039/C4SC00736K.
[46] M. Vázquez López, S.V. Eliseeva, J.M. Blanco, G. Rama, M.R. Bermejo, M. E. Vázquez, J.-C.G. Bünzli, Synthesis and photophysical properties of Ln^{III}–DOTA–Bipy complexes and Ln^{III}–DOTA–Bipy–Ru^{II} coordination conjugates, Eur. J. Inorg. Chem. 2010 (2010) 4532–4545, https://doi.org/10.1002/ejic.201000517.
[47] X. Marset, G. Guillena, D.J. Ramón, Deep eutectic solvents as reaction media for the palladium-catalysed C−S bond formation: scope and mechanistic studies, Chem. Eur. J. 23 (2017) 10522–10526, https://doi.org/10.1002/chem.201702892.
[48] J. Karges, M. Kalaj, M. Gembicky, S.M. Cohen, Re^{I} Tricarbonyl complexes as coordinate covalent inhibitors for the SARS-CoV-2 Main cysteine protease, Angew. Chem. Int. Ed. 60 (2021) 10716–10723, https://doi.org/10.1002/anie.202016768.
[49] P. Kurz, B. Probst, B. Spingler, R. Alberto, Ligand variations in [ReX(diimine)$(CO)_3$] complexes: effects on photocatalytic CO_2 reduction, Eur. J. Inorg. Chem. 2006 (2006) 2966–2974, https://doi.org/10.1002/ejic.200600166.
[50] G.A. Bhat, A.Z. Rashad, T.M. Folsom, D.J. Darensbourg, Placing single-metal complexes into the backbone of CO_2-based polycarbonate chains, construction of nanostructures for prospective micellar catalysis, Organometallics 39 (2020) 1612–1618, https://doi.org/10.1021/acs.organomet.9b00704.
[51] S. Park, S.-H. Moon, T.H. Kim, K.-M. Park, 3,3'-Dimethyl-1,1′-[2,2′-bipyridine-5,5′-diylbis(methylene)]diimidazol-3-ium bis(hexafluorophosphate), Acta Cryst. E 67 (2011) o2392, https://doi.org/10.1107/S160053681103340X.
[52] K. Kalyanasundaram, Luminescence and redox reactions of the metal-to-ligand charge-transfer excited state of tricarbonylchloro-(polypyridyl)rhenium(I) complexes, J. Chem. Soc. Faraday Trans. 2 (82) (1986) 2401–2415, https://doi.org/10.1039/F29868202401.
[53] M. Wrighton, D.L. Morse, Nature of the lowest excited state in tricarbonylchloro-1,10-phenanthrolinerhenium(I) and related complexes, J. Am. Chem. Soc. 96 (1974) 998–1003, https://doi.org/10.1021/ja00811a008.
[54] L.A. Worl, R. Duesing, P. Chen, L.D. Ciana, T.J. Meyer, Photophysical properties of polypyridyl carbonyl complexes of rhenium(I), J. Chem. Soc., Dalton Trans. (1991) 849–858, https://doi.org/10.1039/DT9910000849.
[55] A. Juris, S. Campagna, I. Bidd, J.M. Lehn, R. Ziessel, Synthesis and photophysical and electrochemical properties of new halotricarbonyl(polypyridine)rhenium(I) complexes, Inorg. Chem. 27 (1988) 4007–4011, https://doi.org/10.1021/ic00295a022.
[56] F.P.A. Johnson, M.W. George, F. Hartl, J.J. Turner, Electrocatalytic reduction of CO_2 using the complexes $[Re(bpy)(CO)_3L]^n$ (n = +1, L = $P(OEt)_3$, CH_3CN; n = 0, L = Cl^-, Otf^-; bpy = 2,2′-bipyridine; Otf^- = CF_3SO_3) as catalyst precursors: infrared spectroelectrochemical investigation, Organometallics 15 (1996) 3374–3387, https://doi.org/10.1021/om960044+.
[57] J.M. Smieja, C.P. Kubiak, Re(bipy-^{t}Bu)$(CO)_3$Cl−improved catalytic activity for reduction of carbon dioxide: IR-spectroelectrochemical and mechanistic studies, Inorg. Chem. 49 (2010) 9283–9289, https://doi.org/10.1021/ic1008363.
[58] G.J. Stor, F. Hartl, J.W.M. van Outersterp, D.J. Stufkens, Spectroelectrochemical (IR, UV/Vis) determination of the reduction pathways for a series of $[Re(CO)_3$(alpha-diimine)L'$]^{0/+}$ (L' = halide, OTf^-, THF, MeCN, n-PrCN, PPh_3, P$(OMe)_3$) complexes, Organometallics 14 (1995) 1115–1131, https://doi.org/10.1021/om00003a013.
[59] P. Gerschel, A.L. Cordes, S. Bimmermann, D. Siegmund, N. Metzler-Nolte, U.-P. Apfel, Investigation of cyclam based Re-complexes as potential electrocatalysts for the CO_2 reduction reaction, Z. Anorg. Allg. Chem. 647 (2021) 968–977, https://doi.org/10.1002/zaac.202000450.
[60] E. Šuta, A. Zahirović, V. Tešević, S. Grgurić-Šipka, S. Aranđelović, S. Ljubijankić, J. Ljujić, M. Balaban, A. Hrnjić, A. Višnjevac, N. Ljubijankić, Rare examples of rhenium(I) tricarbonyl iodido complexes with unsymmetrical bipyridines featuring distinguishable rotamers: from synthesis and solid-state/solution-phase isomerism to biological activity, J. Inorg. Biochem. 276 (2026) 113167, https://doi.org/10.1016/j.jinorgbio.2025.113167.
[61] D.N.D. Marcia Cordes, J.L. Walter, Infrared and Raman spectra of heterocyclic compounds—I the infrared studies and normal vibrations of imidazole, Spectrochim. Acta A 24 (1968) 237–252, https://doi.org/10.1016/0584-8539(68)80066-2.
[62] A.N. Hellman, R. Haiges, S.C. Marinescu, Influence of intermolecular hydrogen bonding interactions on the electrocatalytic reduction of CO_2 to CO by 6,6′-amine substituted rhenium bipyridine complexes, ChemElectroChem 8 (2021) 1864–1872, https://doi.org/10.1002/celc.202100306.
[63] B.P. Sullivan, C.M. Bolinger, D. Conrad, W.J. Vining, T.J. Meyer, One- and two-electron pathways in the electrocatalytic reduction of CO_2 by *fac*-Re(bpy)$(CO)_3$Cl (bpy = 2,2′-bipyridine), J. Chem. Soc., Chem. Commun. (1985) 1414–1416, https://doi.org/10.1039/C39850001414.
[64] A.N. Hellman, R. Haiges, S.C. Marinescu, Rhenium bipyridine catalysts with hydrogen bonding pendant amines for CO_2 reduction, Dalton Trans. 48 (2019) 14251–14255, https://doi.org/10.1039/C9DT02689D.
[65] M. Guyot, M.-N. Lalloz, J.S. Aguirre-Araque, G. Rogez, C. Costentin, S. Chardon-Noblat, Rhenium carbonyl molecular catalysts for CO_2 electroreduction: effects on catalysis of bipyridine substituents mimicking anchorage functions to modify electrodes, Inorg. Chem. 61 (2022) 16072–16080, https://doi.org/10.1021/acs.inorgchem.2c02473.
[66] R.C. Knighton, J.M. Beames, S.J.A. Pope, Polycationic Ru(II) luminophores: syntheses, photophysics, and application in electrostatically driven sensitization of

lanthanide luminescence, Inorg. Chem. 62 (2023) 19446–19456, https://doi.org/10.1021/acs.inorgchem.3c02352.
[67] Y. Saga, Y. Nakayama, T. Watanabe, M. Kondo, S. Masaoka, Visible-light-driven hydroacylation of unactivated alkenes using readily available acyl donors, Org. Lett. 25 (2023) 1136–1141, https://doi.org/10.1021/acs.orglett.2c04337.
[68] J.A. Laureanti, G.W. Buchko, S. Katipamula, Q. Su, J.C. Linehan, O.A. Zadvornyy, J.W. Peters, M. O'Hagan, Protein scaffold activates catalytic CO_2 hydrogenation by a rhodium Bis(diphosphine) complex, ACS Catal. 9 (2019) 620–625, https://doi.org/10.1021/acscatal.8b02615.
[69] J.A. Laureanti, B. Ginovska, G.W. Buchko, G.K. Schenter, M. Hebert, O. A. Zadvornyy, J.W. Peters, W.J. Shaw, A positive charge in the outer coordination sphere of an artificial enzyme increases CO_2 hydrogenation, Organometallics 39 (2020) 1532–1544, https://doi.org/10.1021/acs.organomet.9b00843.
[70] C.R. Schneider, H.S. Shafaat, An internal electron reservoir enhances catalytic CO_2 reduction by a semisynthetic enzyme, Chem. Commun. 52 (2016) 9889–9892, https://doi.org/10.1039/C6CC03901D.
[71] X. Liu, F. Kang, C. Hu, L. Wang, Z. Xu, D. Zheng, W. Gong, Y. Lu, Y. Ma, J. Wang, A genetically encoded photosensitizer protein facilitates the rational design of a miniature photocatalytic CO_2-reducing enzyme, Nat. Chem. 10 (2018) 1201–1206, https://doi.org/10.1038/s41557-018-0150-4.